



Gharyan Journal of Technolgy

Annual, Corrected and Accademic Journal

Issued By

Higher Institute of Sciences and Technology, Gharyan

Gharyan - Libya

Issue (10) September 2024

International Code: ISSN (Print) 2518-5993

ISSN (Online) 2521-9308

www.gjt.scitech-gh.edu.ly



Gharyan Journal of Technology
Annual, Reviewed and Academic Journal

Issued By :

Higher Institute of Sciences and Technology, Gharyan

Dr: Melod Mohammed Unis	General Supervision
Dr:Ahmad Ramadan Kobaiz	Editor In Chief
Prof:Abdelati Elalem	Member
Mr: Mohamed Rajab Baiod	Member
Mr:Mohamed M.Alghiryani	Member
Mr:Abdulbasit Mohamad Ali	Member

Contact Us:

: Telephone 0913506053
E-mail: info@gjt.scitech-gh.edu.ly

Contents

English Research Papers	Page
A shunt Compensation Impact on UHVTL Distance Relay using Machine Learning in Discrete Wavelet Classifier Elhadi Emhemed Aker, Mohamed.M.Almelian , Mohammad A Omran and Osajl Emmanuel.	4
Enhancing Strength and Toughness of HSLA Steel Welds through Microalloying with Titanium and Vanadium Addition Musa Moh. H. Abdullrhman, Al-Mehdi M. Ibrahim	22
Multimodal Biometric System Using Dual Digital Watermarking Abdulmawla Najih, Salem s.m Khalifa, Salem Enajeh, Nabila Albannai	49
Comparison of EIGRP, OSPF, and RIP Routing Protocols using OPNET Simulator Aboagela Dogman	80
Video game development on Roblox platform using Lua programming language Sumaia A. Eltomi, Rasheed S. Mottaleb	97

الصفحة	الأوراق البحثية باللغة العربية
12	أثر الرقابة المصرفية في تحسين أداء المصارف الإسلامية الليبية المصرف الإسلامي الليبي نموذجاً محمد عقيل محمد زائد ، جمال محمد فرج ديهوم
47	ما مدى أهمية تطبيق محاسبة الموارد البشرية في الشركات النفطية الليبية هاجر إمحمد الهادي
78	مدى وجود أثر للإفصاح المحاسبي الإلكتروني على جودة المعلومات الواردة في التقارير المالية من وجهة نظر المالىين العاملين المصارف التجارية الليبية في مدينة طرابلس عفاف البهلول ميلود الغضبان

A shunt Compensation Impact on UHVTL Distance Relay using Machine Learning in Discrete Wavelet Classifier

Elhadi Emhemed Aker¹, Mohamed.M.Almelian², Mohammad A Omran³ and Osaj1 Emmanuel⁴.

- 1- Department of Electrical Engineering, Higher Institute of Science and Technology Gharian, Libya
- 2- Department of Electrical Engineering, Higher Institute of Science and Technology Mezdah, Libya
- 3- Faculty of Engineering, College of Technical Sciences, Ben-Walid, Libya
- 4- Department of electrical and electronics Engineering, Federal University Lokoja, Nigeria.

E-Mail: hadi.aker@yahoo.com

الخلاصة:

تقدم هذه الورقة نهجاً ذكياً لاستخراج البيانات لتطوير نموذج تصنيف أخطاء ترحيل المسافة التكيفي للتعلم الآلي (ML-ADR)، باستخدام تحليلات الموجات الهجينة المنفصلة متعددة الحلول وخوارزمية التعلم الآلي (ML- DWMRA) على الجهد العابر للدائرة القصيرة المستخرج ذو الدورة الواحدة. والإشارات الحالية لاكتشاف المعرفة المفيدة المخفية التي يتم نشرها في تعديل ADR الحالي. يتم تشغيل نظام خط النقل، حيث يقوم عنصر المنطقة 3 بالحماية من خطأ الطرف البعيد، مع وبدون نقطة منتصف جهاز تعويض التحويلة المتكاملة على طول الخط. يتم نشر الميزات الـ 29 المستخرجة بشكل فريد عبر 2560 مصدر خطأ من كل من الخطوط المحمية الخاطئة والسليمة لتطوير نموذج تصنيف خطأ ML-ADR من أجل الكشف الفعال عن أخطاء الدائرة القصيرة وتصنيفها وتقليل وقت اتخاذ قرار الرحلة لعنصر الحماية للمنطقة -3. إن النتيجة السابقة من نموذج

مختبر Mat لمرحل المسافة العددية التكيفي المتصل بنظام خط النقل المتكامل لمعوض التحويلة في منتصف النقطة تثبت بالفعل أن وجود تأثير تحت الوصول لخطاً الدائرة القصيرة البعيدة للمنطقة 3 يؤدي إلى تقدير غير صحيح للمقاومة. يوفر ML-ADR أفضل نموذج لتصنيف الأخطاء المتكامل مع أدنى متوسط لقيمة الخطأ المطلق وهو 0.0009، وهذا النموذج راضٍ ويحقق أخيراً أهداف ADR المطلوب.

Abstract

This paper presents an intelligent data mining approach for the Machine Learning-Adaptive Distance Relay (ML-ADR) fault classification model development, using hybrid discrete wavelet multiresolution analyses and machine learning (DWMRA-ML) algorithm on extracted 1-cycle short circuit transient voltage and current signals to discover the hidden useful knowledge that is deployed in the modification of existing ADR. The transmission line system, where the zone-3 element is protecting against the far-end fault is run with and without an integrated shunt compensating device midpoint along the line. The uniquely extracted 29 features across 2,560 fault sources from both faulty and healthy protected lines to build a historical fault database that is deployed for ML-ADR fault classification model development for effective short circuit fault detection, classification, and trip decision time reduction of the zone-3 protective element. The prior result from the Mat lab model of the adaptive numerical distance relay connected on midpoint- shunt compensator integrated transmission line system does indeed establish that the existence of the under-reach effect for zone-3 far-end short circuit fault causes wrong impedance estimation.

The ML-ADR provides the best integrated fault classifier model with the lowest mean absolute error value of 0.0009, this model satisfied and finally meets the objectives of the desired ADR.

Keywords : *Distance Relay, UHV Transmission Line, Discrete Wavelet Transform, Shunt compensation, Zone.*

Introduction

There has been a constant global increase in the amount of electric power energy demands in recent years, these have necessitated the commissioning of new power generation stations, alongside with the expansion of the transmission and distribution grids in meeting these new trends [1] ,[2]. The quest for electrical power energy sustainability solution resulted in the integration of mixed energy generation sources with a high penetration level of renewable energy resources (RERs) in the form of photovoltaic (PVs) and wind turbines (WTs) generation sources on currently existing electric systems to create balances between energy generations and demands [3],[4],[5]. The concerns of evacuations of all generated power from mixed sources to the end load terminals through the transmission and distribution lines are also affected by drops in the voltage values (voltage-sags) at the midpoint of the long-distance transmission lines. These challenges encourage the introduction of Flexible Alternating Current Transmission System (FACTS) devices like the Static Synchronous Series Compensator (SSSC) [6], Static VAR compensator (SVC) [7] , Static Synchronous Compensators [8], and composite compensator like the unified power flow controller (UPFC) [9], for maximum electric power delivery from the generation sources to end-terminal substations at UHV level with minimal power

losses, and voltage variation [10]. These connected FACTS elements on the transmission lines are associated with misoperation challenges to the distance protection relays, by wrong tripping operations due to under-reach and over-reach protection coverage phenomena [11],[12]. Figure 1 displays the transmission line power transfer capability parameters to be considered for optimal transfer of electrical power energy from the source to the load.

Impact of FACTS Devices on Power System Protection

Protection relays are very significant flexible devices used protect the transmission lines and considered as cost-effective, fast response speed and highly reliable [13].

The bottom line of protection devices is discriminating between the normal operating conditions of the power system networks from the abnormal conditions within the allowable limits as stipulated by operating standard to isolate only affected sections from other healthy sections [14], [15]. Transmission line impedances, voltages and currents are the parameters required for protective relay settings and operations. These parameters are, however, significantly affected by FACTS devices installed in the power system. The presence of FACTS devices, therefore, necessitates further investigations on their impacts on the protection scheme layout [16].

FACTS controller's impacts on the performance of distance relays have been a subject of research for the past two decades [17],[18],[19]. Authors in [20], [21], [22] reported that the UPFC and the TCSC have a significant impact on the performance of distance relay in terms of overreach. A general study regarding the influence of

SVC and midpoint shunt compensators on distance relays performance was performed and results were summarized [23].

Research Method

This paper presents a compensated transmission line of 300 km, rated at 400 kV with 50 Hz frequency as depicted in Figure 1. The system under study is a 4-sections system with (A, B, C and D buses) for the 3 protection zones coverage for relay at the sending end bus (A). The system contains generation and load at sending and receiving ends as illustrated in Figure (1). On this study model, various types of faults beyond the compensation device locations are simulated in Matlab software environment for fault voltage and current signals. Valuable data were extracted from each scenario.

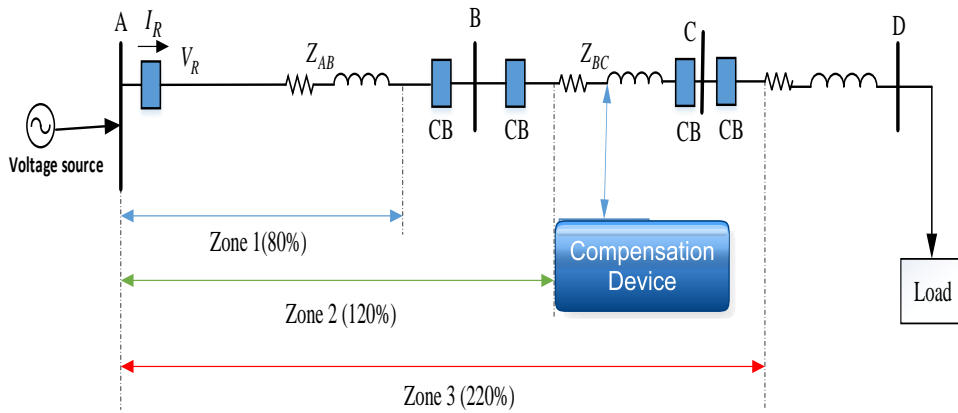


Figure (1): Shunt compensation transmission line

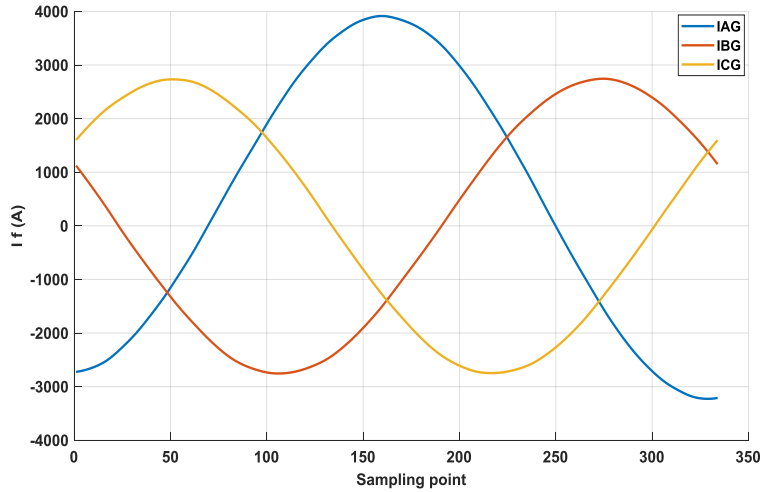


Figure (2): Current waveform for an A-G fault at 200 km
Without integrated shunt compensation

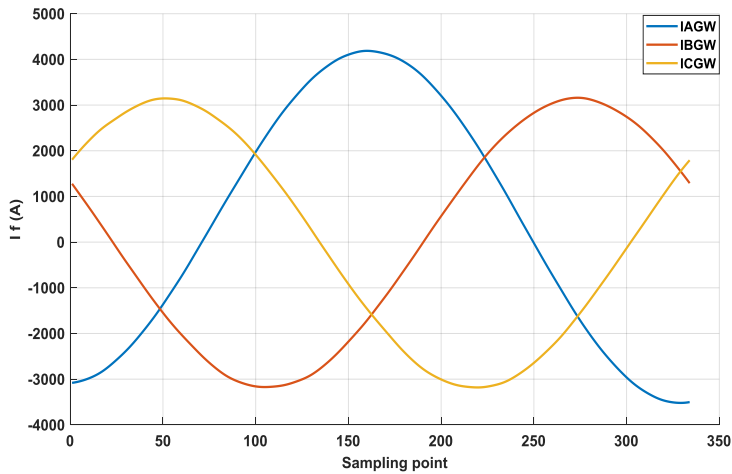


Figure (3): Current waveform for an A-G fault at 200 km
With integrated shunt compensation

Result of Fault Signal Decomposition (DWMRA)

Result from the two proposed power system networks topologies with and without midpoint integrated shunt compensation subjected to ten different fault types from 150 km distance location with the midpoint integrated compensator at 10 km interval to the end of the, under two fault angles (0° C & 30° C), and four fault resistances (0.001Ω , 10Ω , 50Ω , & 100Ω). This produced a three phase-fault transient voltage and current signals across both faulty and healthy lines for short circuit simulations across ten different fault types for a simulation period of 0.2 sec.

The sample of the extracted fault transient current waveform comparison for the phase A-G fault at 200 km far-end fault location without and with integrated midpoint shunt compensation integration on the utility transmission line as displayed in Figures 4 and 5 respectively.

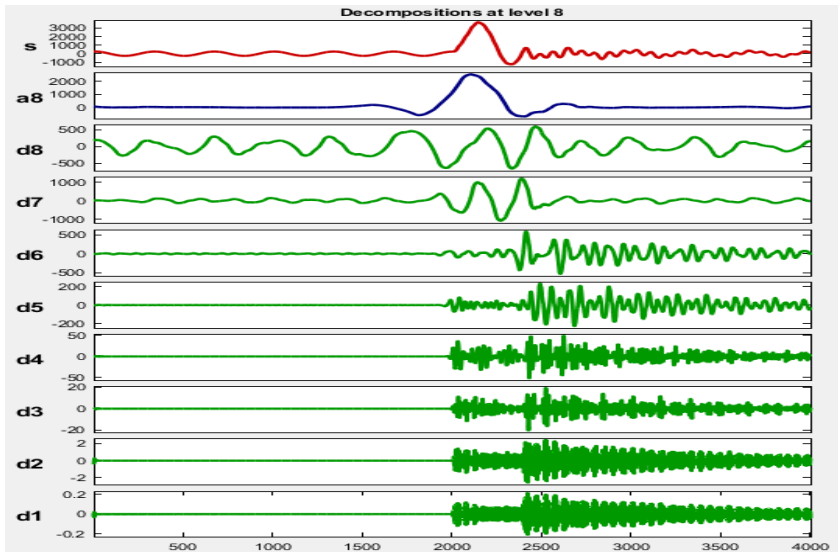


Figure (4): 1-Cycle fault current MRA analysis
Without shunt compensation

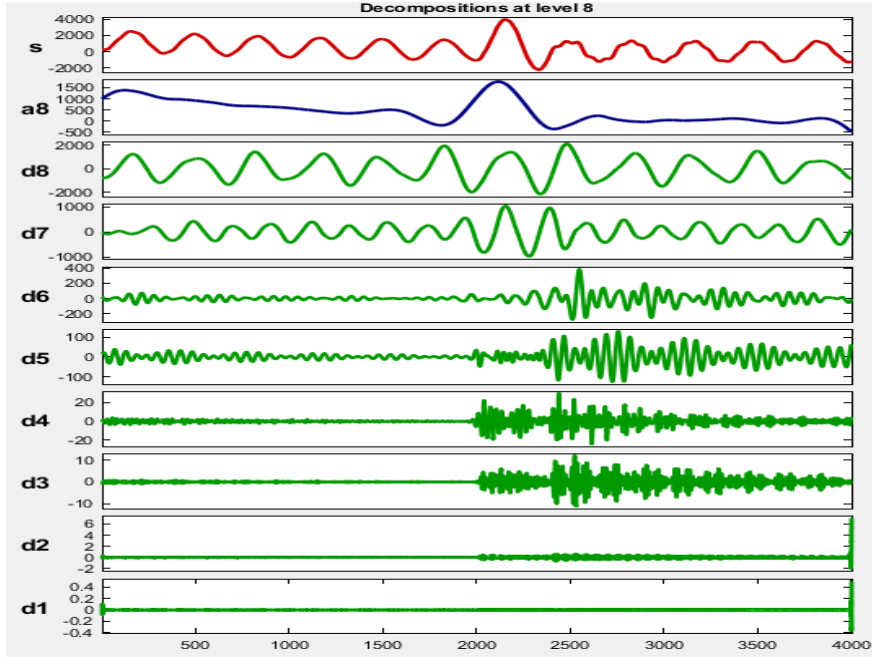


Figure (5): 1-Cycle fault current MRA analysis with shunt compensation

Extracted Features Decomposition Analyses

The hidden useful knowledge of fault signal decomposed parameters are mined for Extraction like the standard deviation (STD), entropy energy value (EE), minimum (min).

The extracted fault transient signals from both voltage and current signals are subjected to 8-levels decomposed DWMRA to extract the useful unique hidden information that may be used in the ML-ADR model development. The samples of the extracted 1-cycle fault transient current decomposition from far-end fault at 200

km are executed for unique feature extraction like the STD, EE, and magnitude with and without midpoint integrated compensation are showed in Figures (2) and (3).

The Discrete Wavelet Transform is a powerful tool for time-frequency signal analysis of sampled localized transient's current signal to produce non-redundant restoration of signal. Moreover, it produces better spatial and spectral localization of signal. In recent decades, such advanced powerful tool has been used for designing the protective relays [17-23]. In DWT, the fault current signal $x(t)$ is decomposed into low and high frequency components such as approximation (A) and detailed coefficients (D) which is mathematically expressed in Equation (1) and (2) for decomposed signal.

$$x(t) = \sum_k cA_1 \Phi_{j-1,k}(t) + \sum_k cD_1 \Phi_{j-1,k}(t) \quad (1)$$
$$x(t) = A_1(t) + D_1(t) \quad (2)$$

The low frequency component of the signal also referred to as the approximation coefficients undergoes series levels of the decomposition up to N level to extract the original information from the noise and for regeneration of the decomposed signal as expressed in Equation (3).

$$x(t) = A_N(t) + D_N(t) + D_{N-1}(t) + \dots D_1(t) \quad (3)$$

Where $N = 5$ is the decomposition level for extracted fault current signals as seen in Figure 6.

WEKA Machine learning and Features Extraction

The Standard Deviation for both model scenarios with compensation device integration or without on the UHV transmission line extracted and analysed accordingly. The under-reach effect occurs only for extracted fault signals at different locations beyond the connected compensation device element for the 3rd zone protection coverage of the distance relay. Other features include the entropy energy of the transient fault signal with hidden related information for fault detection study. All extracted features from transient faults signal are deployed for the onward model building in the WEKA machine learning algorithm for intelligent detective and classification model building scenarios as seen in Figure 6.

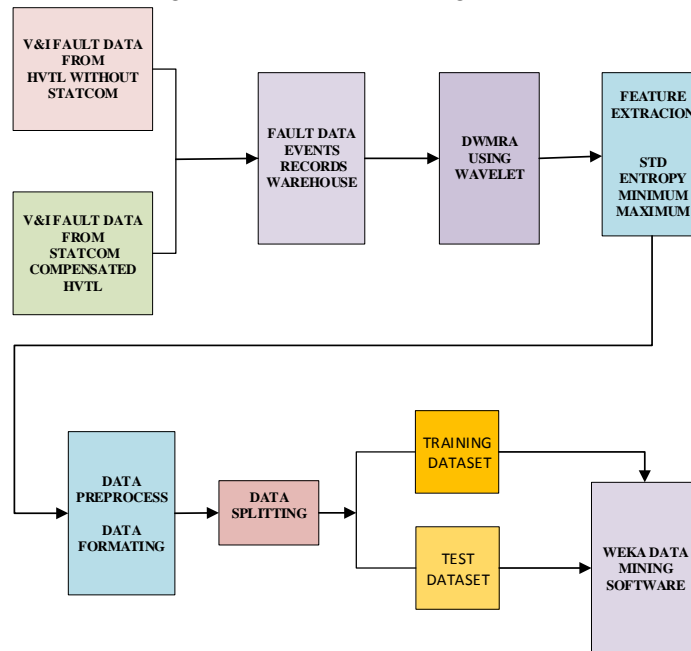


Figure (6): Machine learning (ML) procedure using WEKA software

Results and Analysis

The extracted analyzed result on Table 1 displays the standard deviation for all types of faults, each faulted phase for one scenario without integration of compensation device as proposed. The results displayed no variations under normal operation conditions in the measured current magnitude as showing in figure 2. However, after the integration of compensation, the faulted phase condition as showing in figure 3 is much greater compared to those of healthy lines, thus, indicating a presence of fault. Similarly, there are much differences in the obtained values for integrated scenarios with higher analyzed values of currents for each faulted phases as compared with non-integration scenarios of compensation devices as display in Table 2.

Table (1): Current magnitude during normal conditions and faults at different locations without shunt compensated power system.

Fault Distance	Type of Fault	Without shunt compensator					
		Minimum Current			Maximum Current		
		Ia kA	I b kA	I c kA	Ia kA	I b kA	I c kA
	No fault	-0.205	-0.205	-0.205	0.205	0.205	0.205
100 km	LG	-2.57	-0.34	-0.46	6.95	0.28	0.25
	LL	-4.11	-12.5	-0.25	12.6	4.05	0.25
	LLG	-4.19	-12.0	-0.71	1.34	4.3	0.65
	LLLG	-3.88	-12.0	-12.4	1.52	6.76	4.3
200 km	LG	-1.23	-0.27	-0.39	3.67	0.19	0.18
	LL	-2.19	-7.01	-0.25	7.06	2.16	0.25
	LLG	-2.1	-6.78	-0.45	7.56	2.34	0.38
	LLLG	-1.97	-7.06	-7.16	8.32	3.78	2.82
300 km	LG	-0.78	-0.294	-0.37	2.49	0.185	0.19

	LL	-1.56	-4.78	-0.25	4.93	1.47	0.25
	LLG	-1.51	-4.85	-0.51	5.08	1.62	0.37
	LLLG	-1.31	-5.17	-4.97	5.72	2.62	2.16

Table (2): Current magnitude during normal conditions and faults at different locations with shunt compensated power system.

Fault Distance	Type of Fault	With shunt compensator					
		Minimum Current			Maximum Current		
		I a kA	I b kA	I c kA	I a kA	I b kA	I c kA
	No f	-1.22	-2.07	-2.08	2.51	1.26	1.21
100 km	LG	-3.36	-1.04	1.17	6.95	1.23	0.8
	LL	-4.57	-11.7	-1.24	11.8	4.58	1.07
	LLG	-4.74	-11.4	-1.3	1.26	4.82	1.18
	LLLG	-4.57	-11.5	-1.1.9	1.43	7.02	4.91
200 km	LG	-2.20	-1.12	-1.23	3.97	1.23	1.08
	LL	-2.80	-6.3	-1.25	6.38	2.71	1.07
	LLG	-2.85	-6.25	-1.36	6.76	2.99	1.09
	LLLG	-2.72	-6.47	-6.46	4.49	4.06	3.3
300 km	LG	-1.85	-1.19	-1.28	3.18	1.22	0.84
	LL	-2.22	-4.56	-1.27	4.61	2.22	1.07
	LLG	-2.33	-4.61	-1.38	4.88	2.41	1.17
	LLLG	-2.22	-4.84	-4.79	5.32	3.24	2.68

Furthermore, the entropy energy result in Table 2 displays the similar information for the normal conditions without variations in the current values under both simulation scenarios. The faulted phase entropy energy value is higher across all faulted phases as an indication of fault presence. The comparison study also indicated a much higher value in entropy energy under integrated compensation device

condition as compared to non-integration as highlighted in red on the displayed results.

The analyses performances of the fault classification models developed in WEKA to address the pending under-reach challenges encountered by distance relay for 3rd zone's fault detection on a compensation device line indicated effective model performance with the deployment of the propose Naive ML-ADR algorithm as compared to other intelligent algorithm with 100% accuracy for all most fault detection and discrimination as observe in Table 3.

ML-ADR Classifier Model Validation

The evaluated ML-ADR model addresses the impeding zone-3 element trip operation compromise is further validated by deploying into the new set of extracted real-life simulation data that was not used in the model training and testing. To validate all developed fault classifier models to determine the performance generalization of the model with the new fault scenarios data acquisition from different fault types different from those applied in the model training and testing across both proposed models. Several random sampled transient short circuit faults were deployed for the validation study. The summary of the new extracted and validation dataset that are pre-processed similarly as the training and test dataset deployed in the ML-ADR classification model at different faults in Table 3.

Table (3): ML-ADR classifier model validation result

Fault Classifier Models	Faults Instance Record	Correctly Classified	Incorrectly Classified	Model Performance (%)	Mean absolute error	ROC Area (%)
ML-ADR-LG	194	194	0	100	0	1
ML-ADR-LLG	192	188	4	97.91	0.0069	1
ML-ADR-LL	190	190	0	100	0	1
ML-ADR-LLLG	62	60	2	96.77	0.0277	1
Integrated ML-ADR	638	632	6	99.06	0.0009	1

Conclusion

The adoption of an appropriate machine learning (ML) intelligent algorithm model studies the adaptive distance relay (ADR) modelling that should eliminate the zone-3 protective element compromise during far-end fault due to under reach effect from midpoint integrated shunt compensator on transmission lines. This has been successfully achieved. The study has addressed the impending distance relay

zone-3 element backup protection compromise due to under reach effect caused by the infeed contribution of the short circuit current from the shunt compensator into the faulty section of the transmission lines.

The deployed integrated ML-ADR fault classifier model is successfully deployed using decomposed extracted 2,560 historical fault database records from 1-cycle fault voltage and current signal in combination with network topology variations.

References

- [1] Petinrin, J. and M. Shaabanb, Impact of renewable generation on voltage control in distribution systems. *Renewable and Sustainable Energy Reviews*, 2016. **65**: p. 770-783.
- [2] Hariadi, T.K., et al., Energy efficiency and policy analysis for household in DI Yogyakarta (Yogyakarta Special Region) Indonesia. *International Journal on Advanced Science, Engineering and Information Technology*, 2016. **6(3)**: p. 329-333.
- [3] Liserre, M., T. Sauter, and J.Y. Hung, Future energy systems: Integrating renewable energy sources into the smart power grid through industrial electronics. *IEEE industrial electronics magazine*, 2010. **4(1)**: p. 18-37.
- [4] Naserian, M., A. Karimi, and S.E. Mirabdolahi, Robust Optimal Controller Design for Induction Generator Driven by Variable-Speed Wind Turbine with STATCOM Using Immune Algorithm. *International Journal on Advanced Science, Engineering and Information Technology*, 2011. **1(5)**: p. 481-486.

- [5] Samir, A., et al., Efficient PV-grid system integration with PV-voltage-source converter reactive power support. The Journal of Engineering, 2018. **2018**(2): p. 130-137.
- [6] Zellagui, M. and A. Chaghi, Effects of shunt FACTS devices on MHO distance protection setting in 400 kV transmission line. Electrical and Electronic Engineering, 2012. **2**(3): p. 164-169.
- [7] Khoa, N.M. and D.D. Tung, Locating fault on transmission line with static var compensator based on phasor measurement unit. Energies, 2018. **11**(9): p. 2380.
- [8] Rabie, S. and H. Afrakhte, Optimal determination of island boundaries besides the optimal placement of D-STATCOM devices and DG units. Turkish Journal of Electrical Engineering and Computer Sciences, 2017. **25**(2): p. 1508-1521.
- [9] Al-Behadili, A.K.L., Performance Analysis of Distance Relay on Shunt/Series Facts-Compensated Transmission Line. 2015.
- [10] Moravej, Z., M. Pazoki, and M. Khederzadeh, New smart fault locator in compensated line with UPFC. International Journal of Electrical Power & Energy Systems, 2017. **92**: p. 125-135.
- [11] Gupta, O.H. and M. Tripathy. Relaying scheme for STATCOM compensated transmission line. in 2016 IEEE 6th international conference on power systems (ICPS). 2016. IEEE.
- [12] Ilango, R., Impact Analysis of midpoint Connected STATCOM on Distance Relay Performance. TELKOMNIKA Indonesian Journal of Electrical Engineering, 2015. **13**(2): p. 257-263.
- [13] Yadav, A. and Y. Dash, An overview of transmission line protection by artificial neural network: fault detection, fault classification, fault location, and fault

- direction discrimination. *Advances in Artificial Neural Systems*, 2014. **2014**(1): p. 230382.
- [14] Purohit, M. and V. Gohokar, Effects of series compensation on distance protection of high voltage transmission lines under fault conditions. *International Journal of Electrical Engineering & Technology (IJEET)* Volume. **9**: p. 57-66.
- [15] Gopakumar, P., M.J.B. Reddy, and D.K. Mohanta, Transmission line fault detection and localisation methodology using PMU measurements. *IET Generation, Transmission & Distribution*, 2015. **9**(11): p. 1033-1042.
- [16] 16.Ghorbani, A., B. Mozafari, and A.M. Ranjbar, Digital distance protection of transmission lines in the presence of SSSC. *International Journal of Electrical Power & Energy Systems*, 2012. **43**(1): p. 712-719.
- [17] 17.Behera, S., P. Raja, and S. Moorthi. Modelling and simulation of the impact of SVC on existing distance relay for transmission line protection. in *2015 International Conference on Condition Assessment Techniques in Electrical Systems (CATCON)*. 2015. IEEE.
- [18] 18.Gupta, O.H. and M. Tripathy, An innovative pilot relaying scheme for shunt-compensated line. *IEEE transactions on power delivery*, 2015. **30**(3): p. 1439-1448.
- [19] 19.Chandan, A., et al., Advance distance protection of transmission line in presence of shunt compensator. *International Research Journal of Engineering and Technology (IRJET)*, 2015. **2**(3): p. 751-757.
- [20] 20.Reyes-Archundia, E., E. Moreno-Goytia, and J. Guardado, An algorithm based on traveling waves for transmission line protection in a TCSC environment. *International Journal of Electrical Power & Energy Systems*, 2014. **60**: p. 367-377.

- [21] 21.Hemmati, R., M. Nikzad, and S.S.S. Farahani, Investigation of UPFC performance under system uncertainties. International Journal of Electrical Power & Energy Systems, 2012. **43**(1): p. 1137-1143.
- [22] 22.Mehrjerdi, H. and A. Ghorbani, Adaptive algorithm for transmission line protection in the presence of UPFC. International Journal of Electrical Power & Energy Systems, 2017. **91**: p. 10-19.
- [23] Hemasundar, D., M. Thakre, and V. Kale. Impact of STATCOM on distance relay-Modeling and simulation using PSCAD/EMTDC. in 2014 IEEE Students' Conference on Electrical, Electronics and Computer Science. 2014. IEEE.

Enhancing Strength and Toughness of HSLA Steel Welds through Microalloying with Titanium and Vanadium Addition

Musa Moh. H. Abdullrhman¹, Al-Mehdi M. Ibrahim²

1- dept. of Petroleum Engineering University of Gharyan Gharyan, Libya
mosa.hossin@gu.edu.ly

2- dept. of Mechanical & industrial Eng. University of Gharyan Gharyan, Libya
al-mehdi.ibrahem@gu.edu.ly

المخلص

تهدف هذه الدراسة إلى تحسين قوة ومثانة منطقة اللحام للصلب عالي القوة ومنخفض السبائك (HSLA) عن طريق إضافة عناصر السبائك الدقيقة والمتمثلة في التيتانيوم والفاناديوم عبر تقنية لحام شعلة غاز التنجستن الخامل. تم إجراء إذابة العناصر المضافة للحام باستخدام المسحوق المسبق مع متغيرات اللحام للتيار 80-100 أمبير والجهد 30-40 فولت. أظهرت نتائج الأختبارات المعملية أن عناصر Ti و V تلعب دورا هاما في خصائص المنطقة المتأثرة بالحرارة (HAZ)، وصلابة الصدمات، وقوة الشد للفولاذ HSLA. علاوة على ذلك، تم تحقيق أقصى قوة شد (UTS) بلغت 693 ميغا باسكال و 730 ميغا باسكال مع إضافة كل من Ti و V على التوالي. كما لوحظ الانخفاض في قيم صلادة HAZ مع إضافة Ti و V 15% و 19% على التوالي، مقارنة بلحام السبيكة بدون إضافات، مما يقلل من خطر الكسور المفاجئة والهشة التي تحدث في المنشآت الصناعية وتسبب خسائر بشرية وإقتصادية.

Abstract

The study aims to improve the strength, and the toughness of the welding zone of high strength low alloy steel (HSLA) by adding microalloying elements, titanium, and vanadium via tungsten inert gas torch technique. The melting was carried out using powder preplacement procedure with the welding variables of current, 80-100A and voltage, 30-40V. Experimental results showed that Ti and V elements play an

important role on the heat affected zone hardness, impact toughness and tensile strength of HSLA steel. Furthermore, a maximum ultimate tensile strength of 693 MPa and 730 MPa were achieved with Ti and V addition respectively. The reduction in HAZ hardness values with Ti and V addition was 15% and 19% respectively, compared to base material, thereby reducing the risk of brittle fracture.

Keywords

High strength low alloy steel, Ti and V microalloying elements, heat affected zone, microstructure and mechanical properties.

1. Introduction

The design of high strength low alloy (HSLA) steels play an important role in structural performance which can easily be done with their performance properties such as, lower structural thickness, weight, and load-bearing capacity. This in turn can provide an excellent balance between strength, toughness, ductility, formability, and weldability in contrast to conventional carbon steels [1-3]. In recent decades, much steel research and development efforts have focused on HSLA. The application of this kind of steel has expanded to various industries including shipbuilding, oil and gas pipelines, building, storage tanks, pressure vessels, high strength fasteners and suspension springs after its initial application in the automobile industry.

This is due to its high strength-to-weight ratio, excellent weldability, formability, and cost reduction [4, 5]. In most of the cases, welding is indispensable to use HSLA steel for any application. There are major challenges associated with the welding zones for this type of steel, and the welding processes which have a significant effect on the integrity of the welded structures and their performance in service. The main problem associated with this HSLA steel is to obtain a good combination of strength, toughness, and weldability properties specifically in a welded zone which includes grain coarsening in and around the region of the weld [6]. Furthermore, due to a longer thermal cycle and slower cooling rate, formation of martensitic in weld section and precipitation of carbides at the grain boundaries cause poor mechanical properties in HAZ and hence, lead to several fracture problems [7, 8].

The desired welding variables are selected based on the data available in handbook or experience of the users. However, it might not be accurate for achieving optimum characteristics feature of HAZ or welded zone for wide range of applications. Moreover, it is very difficult to optimize the welding variables because of the complex interaction of the melt pool during welding process. This probably explains why the issue persists and not much has been achieved [9]. Another problem associated with the HSLA steel is the brittleness related to the formation of high carbon martensite-austenite (M-A) and prior austenite grains (PAG) constituents along the grain boundaries which located in the HAZ and the fracture behavior of HAZ developed due to low ductility and low notch impact toughness of HAZ material [10].

These fractures are initiated mostly from second phase particles and inclusions and lead to catastrophic failure related to injury or fatality of humans and the loss of national assets [11, 12]. These losses of toughness properties in HAZs constrain the wide application of high strength steel. It is thus required to understand how to minimize the risks resulting from welding zones and the behavior of the HAZ which determines the efficiency of the entire welded joint. During the past decades, investigations on the morphology and mechanical properties of the HAZ in welding of HSLA steels have focused on finding several practical solutions to prevent sudden fractures in welding zones during their service conditions [13, 14].

It is necessary to find an alternative method to reduce and overcome these risks in the metallurgical and weldability issues related to the HAZ associated with the welding processes of these types of steels to improve the structure and properties of the HAZ. The addition of microalloying elements through small quantities of Ti and V play a vital role for performance property and structural integrity of HSLA steels [15]. These alloying elements have the high affinity to carbon and nitrogen which can greatly influence the new microstructure formation such as by carbide or nitride precipitates. However, these precipitates are in generally complex and the Ti, and V as well as C and N are all interchangeable depending on the formation temperature. Furthermore, stable Ti-rich carbonitrides can work negatively by constricting austenite grain coarsening during austenitization and V-rich carbides promote precipitation hardening during cooling [16-18].

Maduraimuthu et al. [19] have performed parametric optimization of TIG welding using Taguchi design method for P92 (9Cr-0.5Mo-1.8W-VNb) Steel by using response surface methodology and emphasized on the optimization of process parameters in welding process. However, addition of these microalloying elements would be better choice to avoid the problems associated with brittle fractures and environmental degradation occurring in welding zones. Based on the literature, it is evident that weld parameters influence the strength, toughness, and microstructure of HSLA steel, but the results are still insufficient in finding ideal solutions due to the continued deterioration of weld properties, and catastrophic failure occurring particularly in the HAZ area. Furthermore, little research has been done on the microalloying elements addition and its effects on mechanical properties and microstructures performance of HAZ for HSLA steel.

Therefore, the main aim of this study is to explore the addition of Ti and V microalloying elements on the improvement of metallurgical and mechanical performance of HSLA steel. Implementing this optimized TIG welding parameters can be benchmark for welding companies as TIG welding is an international welding concept. This can attract end-users to exploit this approach of HSLA steel with improved metallurgical and mechanical performance avoiding catastrophic failure.

2. Experimental Method

2.1 Material

HSLA steel with L450 specifications was used in this investigation in the form of 10 mm thickness plate was cut and machined to accomplish thin plate specimens of dimensions 150 mm x 50 mm x 5 mm. The chemical composition and mechanical properties of HSLA steel are presented in Table 1 and 2, respectively and details of the measurement procedure can be found elsewhere [21]. The surface of the specimens was cleaned in a Branson 2510 ultrasonic cleaner for duration of 10 min. For experiments with microalloying element preplacement, the substrate surfaces were ground by 180 grit emery paper to have better retention of the preplaced powder.

Table 1: Chemical composition of L450 steel (wt. %) [21]

C	Si	Mn	S	P	Al	V	Nb	Ti	Fe	*C _{eq}
0.08	0.17	1.41	0.014	0.0017	0.032	0.022	0.019	0.015	Bal.	0.38

$$*C_{eq}: CE = (\%C) + (\%Mn/6) + (\%Cr+\%Mo+\%V)/5 + (\%Cu+\%Ni)/15$$

Table 2: Mechanical properties of raw L450 HSLA steel [21]

Steel Grade	Yield strength Y.S, MPa	Tensile strength UTS, MPa	Elongation, %	Impact toughness, J	Hardness, Hv0.5
L450	450-500	550-600	35	105	175

Microalloying elements

Ti microalloying element in the form of powder with average particle size, 45 μm, 99.70 wt. % purity, and V microalloying element in the form of powder with average particle size of 45 μm, 99.45 wt. % purity was selected as reinforcing microalloying elements to act as grain refining elements in HSLA steel welds [22, 23]. These elements were added as alloying elements during the welding process. A different approach was adopted to add these microalloying elements only in the weld pool, and not in the bulk material using a powder preplacement technique. The range of individual microalloying element powders used in this study was determined through a preliminary investigation and through previous studies [24, 25].

Polyvinyl Alcohol Binder

The polyvinyl alcohol (PVA) is an organic binder mixed with distilled water in the ratio of 40 grams of PVA to 960 ml of water to prepare one liter of 4% PVA. The mixture was then heated stirring occasionally until a clear solution was obtained, which was stored and used for the preplacement of the microalloying element. It is effective in film forming and has a strong adhesive quality. It is characterized by properties such as chemical resistance; water solubility and it can chemically bind with a nanoparticle surface [26].

2.2 Test equipment

Several equipment and machines were used to produce and investigate the welding heat affected zone of welded HSLA. The machining of HSLA steel substrate was carried out using Milling and EDM- W11FX2K wire cut machines. Miller-Telwin 165-TIG welding machine was used to produce welding tracks. JEOL, JSM-IT100 scanning electron microscope (SEM) integrated with energy dispersive X-ray (EDX) was used to characterize the microstructures and the morphology of heat affect zone (HAZ) of welding region, and to detect the elemental compositions. Phase identification was conducted using Shimadzu 6000 XRD diffractometer.

Instron SI-1C3 300FT-LBS Impact testing machine and Mitutoyo MVK-H2 digital microhardness testing machine were used for impact toughness and hardness measurements, respectively. Instron 5582-100KN universal testing machine was used for tensile testing. The arc generated by the TIG torch welding process using non-consumable tungsten electrode under different welding variables was adapted for the realization of powder melting by reinforcing microalloying elements in the form of powder on the melt pool of HSLA steel. The TIG arc process allows localized heat source that established between a pointed non-consumable tungsten electrode and the substrate materials.

A 3.2 mm diameter tungsten electrode with 2% thorium was selected for the TIG torch used in this study. The electrode has good current carrying capacity, and resistance to contamination the arc generated was more stable. Argon gas with a flow rate of 20 l/min was used to create an inert environment during the TIG melting process due to its advantageous characteristics. These advantages offered a clean, small, and robust joint weld, suitable for most applications. It gives more energy imparted to the surface of the metal and gives deeper penetration than other shielding gases.

2.3 Methodology

The experiments were conducted by preparing Ti and V microalloying elements powder reinforced on the surface of L450 HSLA steel substrates. The surface melting experiment was achieved using powder replacement procedures and TIG torch melting techniques under a non-oxidizing atmosphere. For a comparison with the modified welded specimens with the addition of microalloying element, the sample of

the base material was welded using the same input parameters without microalloying addition.

Preparation of preplaced microalloying element on HSLA steel substrate

The first step of the welding modification process was to prepare the microalloying element powder material on the surface of L450 HSLA steel as a substrate material using the powder preplacement approach. Before applying the microalloying element powder, the surface of the substrate sample was abrasively ground to a smooth surface roughness using silicon carbide (SiC) emery paper. The grounded substrates were subsequently rinsed with acetone followed by ethanol in an ultrasonic bath for 20 minutes.

This treatment removed impurities such as grease, dust, and oxide layer from the substrate surface. Two types of microalloying element powders namely Ti and V were selected for welding modification in this study via melting in the weld pool through the welding of HSLA steel substrate. The amount of microalloying element was a primary variable, while the powder types were used as the categorical variables as presented in Table 3.

All results are average from three measurements. Before preplacement process, each microalloying element powder was weighed using 1.0 mg/mm² of the substrate surface which was made in a pasty form after mixing of PVA, distilled water and alcohol. The pastes of the microalloying element were evenly preplaced on the HSLA steel surface with the aid of a plastic sheet. PVA was used to prevent the powders from blowing away due to the shielded Ar gas flow during melting process. The minimum quantity of PVA was used with a thumb rule of 0.5 ml for 2.0 mg of powder to avoid porosity development on the re-solidified layer of the steel [26, 27]. Finally, the preplacement surfaces with thickness layer of about 0.5-1.5 mm were dried in an electric oven at 70 °C for 1 hr to remove any moisture.

TIG melting of preplaced microalloying element on HSLA steel substrate

The melting of the dry preplaced surfaces was carried out beneath a direct current electrode negative (DCEN) arc of TIG welding machine to produce a series of autogenous weld tracks on the previously prepared substrates. The experimental setup, powder preplacement and welding track development using TIG torch melting process of HSLA steel is shown in Fig. 1.

Table 3 Design matrix and responses for TIG torch processing of HSLA steel without and with microalloying element (Ti, V) addition.

Exp. Run	Parameters			Responses								
	A	B	C	Hardness (Hv0.5)			Impact toughness (J)			Tensile strength (MPa)		
	Welding current (A)	Welding voltage (V)	Ti or V microalloy element (mg/mm ²)	No alloy	Ti	V	alloy No	Ti	V	alloy No	Ti	V
1	80	30	1	293	246	233	41	58	68	605.05	675.4	669.4
2	90	35	1	264	234	202	48	69	72	704.30	611.7	693.2
3	100	40	1	242	226	217	50	77	75	653.00	644.9	688.0
4	80	35	1.5	273	225	225	43	68	72	611.36	685.8	729.8
5	90	40	1.5	250	223	208	47	81	69	641.80	692.9	635.4
6	100	30	1.5	265	202	206	44	78	76	644.06	635.4	714.3
7	80	40	2	259	211	218	40	53	74	611.81	676.8	596.0
8	90	30	2	287	239	213	42	66	68	665.43	686.8	700.3
9	100	35	2	255	250	223	49	63	72	670.79	601.0	699.2

*Fixed parameters (Argon flow rate= 20 l/min and welding travel speed= 1.0 mm/s).

The melt pool for the process was created by striking a metal arc between the tip of a throated tungsten electrode (3.2 mm diameter) and the steel substrate. The arc produced was controlled using an arc gap length maintained at 2 mm while the welding speed was controlled through externally loaded software interface attached to the welding machine. The TIG process was conducted under the streamed argon gas at 20 l/min, which was channeled through electrode gun to prevent oxidation of the

molten surface layer during the melting process. The detailed specifications for the TIG melting conditions are provided in Table 4.

Table 4 Details of TIG melting process parameters

Current (A)	80-100 with increment of 10 A
Current frequency (Hz)	20 Hz
Speed (mm/s)	1.0 mm/s
Voltage (V)	30-40 with increment of 5V
Electrode configuration	3.2 mm, W-2%. Th., 60° cone included angle
Arc gap (mm)	2.0 mm
Argon flow rate (ml/min)	20 l/min
Specimen position	Flat
Torch orientation	Vertical
Process	DCEN

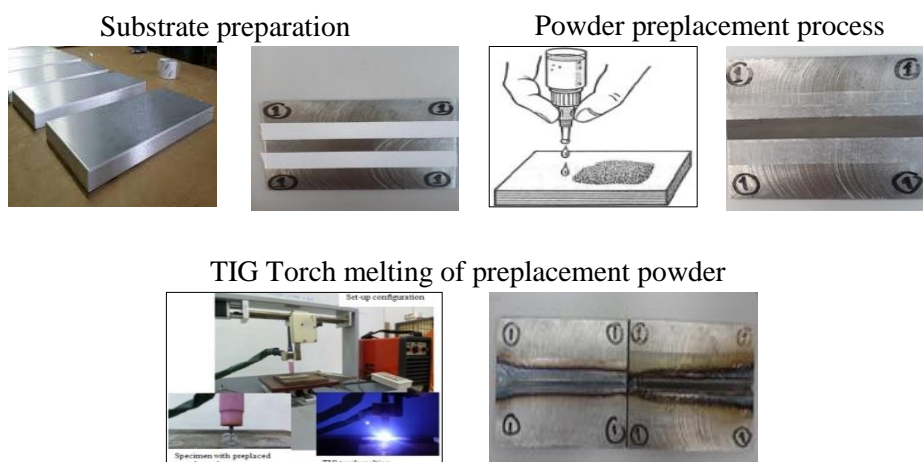


Figure 1: Powder preplacement and welding track Development

The TIG torch welding was carried out using a range of heat input from 1152 to 1920 J/mm and shielded by argon delivered at a rate of 20 l/min.

$$\text{Heat input, } E = \eta IV / S \quad (1)$$

Eq. 1 was used to calculate the heat input (E), where V and I are the voltage and current, respectively, and s is the scanning speed of the torch in melting a track across the prepositioned powder sample. The symbol η is the efficiency for energy absorbed in the sample and was designated elsewhere [28] as 48%. The process parameters including control factors are provided in Table 4.

The WOLPERT WILSON Vickers microhardness testing machine was used for the material 200 hardness measurement with an indentation load range 500 gf for dwell time of 10 seconds. Hardness profiles were measured both from the beginning and along the depth of the transverse sections of the HAZ. Microhardness measurements taken from the center were performed at a depth of about 300 μm away from the surface region and these were conducted for all the samples under parametric study using L9 Taguchi array.

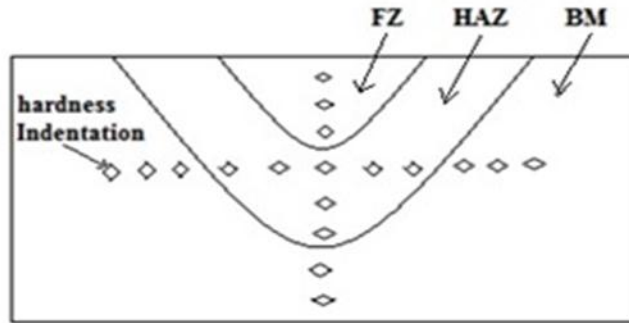


Fig.2: Schematic diagram showing the path of hardness measurements of the weld; FZ: Fusion zone, HAZ: Heat affected zone, BM: Base metal.

The hardness measured for the performance analysis of modified welded HSLA steel after optimization process was conducted across the HAZ at an interval of 200 μm . The microhardness values were the average of five readings taken from the respective interval depth. Fig. 2 shows the hardness indentation track of the welded zones. Samples for impact toughness were cut and prepared from the welding area specifically in HAZ by means of wire cutting machine. Charpy V-notch impact test was performed at room temperature using an INSTRON-SI-1C3 universal pendulum

impact tester on the sub-size specimens, shown in Figs. 3 (a), (b), and (c) following ASTM E23-02a guidelines.

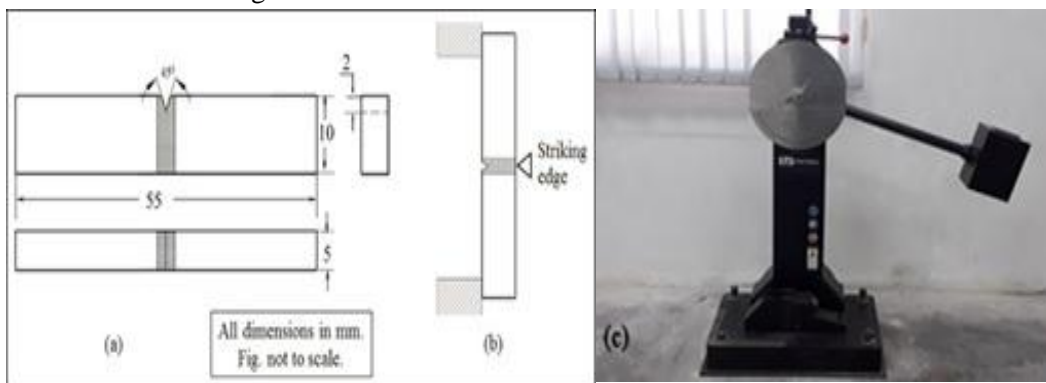


Fig. 3: (a) ASTM E23 proportions of Charpy V-notch specimen, (b) Position of specimen during the test, and (c) Impact testing machine.

The tensile test was conducted on the specimens by pulling transversely to the weld line in accordance with ASTM E8/E8M–11 to determine the tensile strength of the material.

3. Results and discussion

3.1 X-ray diffraction (XRD) analysis on HAZ of HSLA steel

The phase identification of substrate HSLA steel was performed using X-ray diffraction (XRD) technique. Fig. 4(a) shows a typical X-ray diffraction pattern for the un-welded HSLA steel. The diffraction peaks at 45° , 65° and 82.3° corresponded to the $\alpha(110)$, $\alpha(200)$ and $\alpha(211)$ phase respectively, whilst the peaks at 37.5° , 43° and 54.5° indicated the presence of pearlite $\text{Fe}_3\text{C}(112)$, $\text{Fe}_3\text{C}(121)$ and $\text{Fe}_3\text{C}(211)$ phase respectively in the HSLA steel raw material 225 with low intensity. The XRD spectrums of TIG torch welded HSLA steel with Ti and V microalloying addition are shown in Figs. 4(b) and 4(c) respectively. The precipitates of intermetallic compounds formed in the HAZ of welded HSLA steel are identified in the figures, corresponding to TiN, TiC and TiS for Ti microalloying element addition (Fig. 4b) and VN, VC and VS for V addition (Fig. 4c).

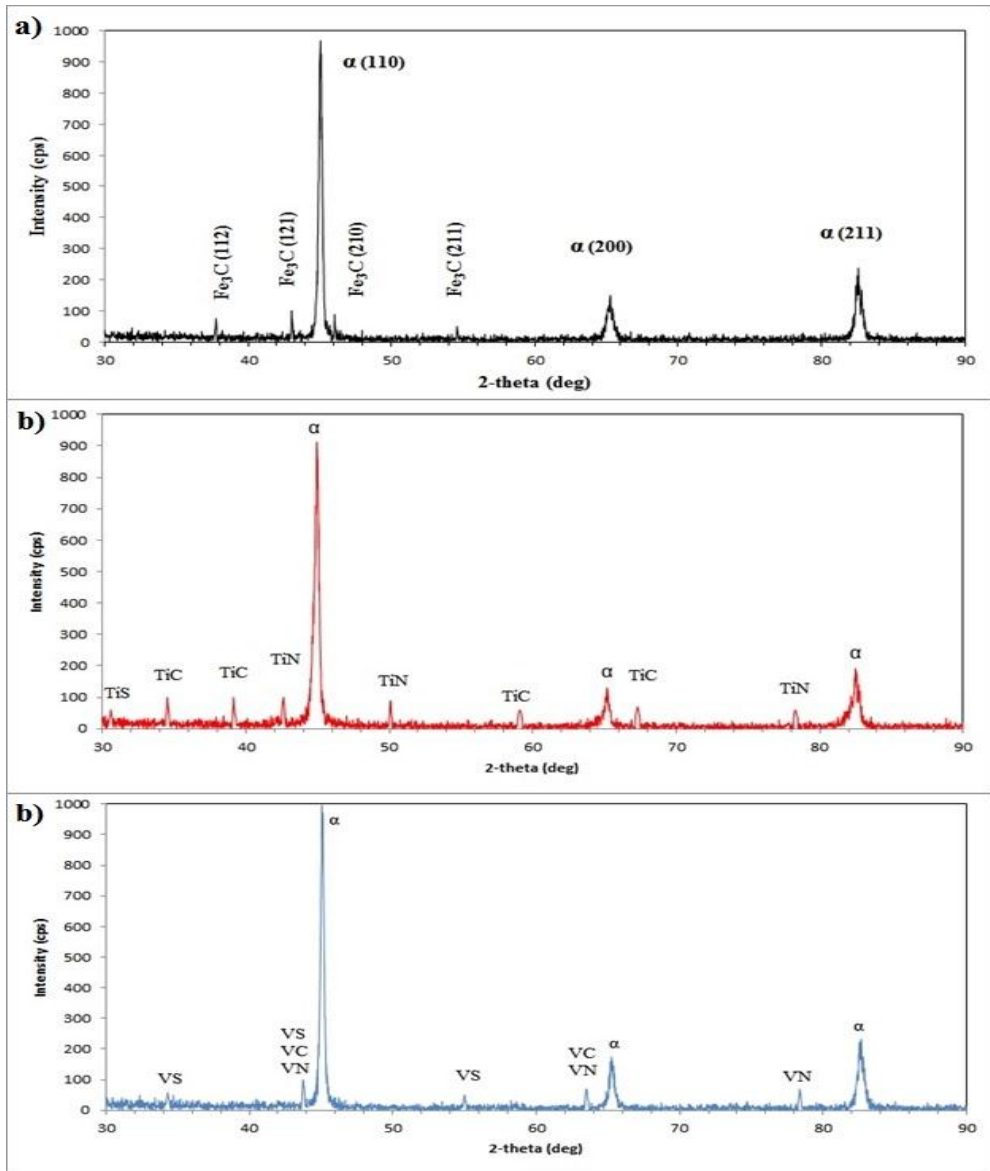


Fig. 4: XRD spectrum of (a) L450 substrate material, (b) TIG torch welded HSLA steel with Ti addition, (c) TIG torch welded HSLA steel with V addition.

3.2 Effect of microalloying elements addition on microstructure

The significant reduction in the HAZ hardness, and enhancement in the tensile strength and the impact toughness of welded HSLA steel is associated with the presence of carbonitride forming microalloying elements Ti and V in the newly formed microstructure which can considerably mitigate the negative influence of welded zones on the mechanical properties and microstructure for HSLA steel. The microstructure of the as-received HSLA steel showed the nature and morphology of the grain structure and distribution of other intrinsic features in the microstructure. Fig. 5 shows the ferrite and pearlite phases that distributed along the diffraction angle within the range of $30^\circ - 90^\circ$, see Fig. 4(a)

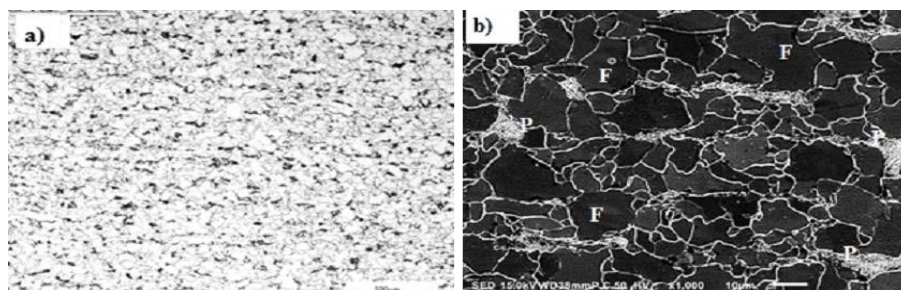


Fig. 5: (a) Optical microstructure and (b) SEM microstructure of HSLA steel L450 substrate material.

The microalloying element, particularly Ti is mainly used to reduce the grain size and to ensure grain refinement because austenite grain growth is retarded by titanium nitride. It is worthy to mention that the best Ti amount for obtaining precipitates should be small enough to accelerate the pinning effect on the austenite grain boundaries as the higher amount of Ti has adverse effect on the formation of coarse precipitates. The developed precipitates are known for higher hardness but make the welded material brittle as reported by [29, 30]. The addition of Ti accelerates the transformation of austenite to ferrite and modifies the morphology of ferrite from Widmanstätten ferrite (WF) to acicular ferrite (A-F). The microstructural evolutions of the HAZ of HSLA steel with 1.0 mg/mm^2 Ti microalloying element addition were characterized via scanning electron microscopy (SEM). Fig. 6 shows the HAZ microstructure of melted HSLA steel with 1152 J/mm heat input. At lower heat input

range, the influence of heat input and microalloying element addition on the mechanical properties are both significant, see Figs. 7-9.

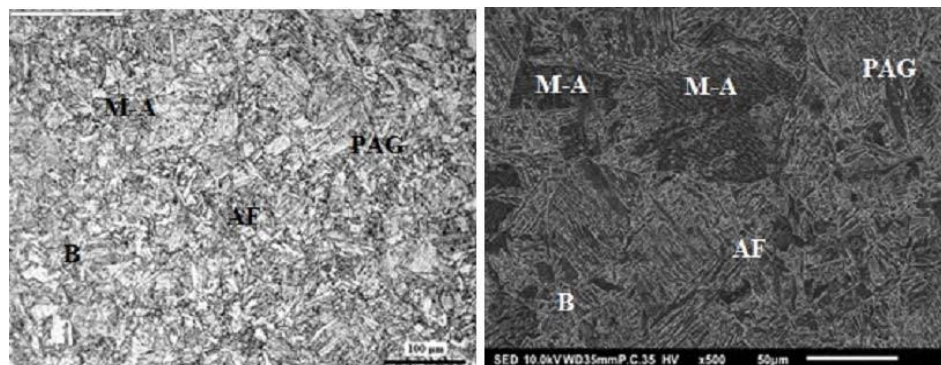


Fig. 6: OM and SEM micrographs of HAZ of welded HSLA steel with 1.0 mg/mm^2 Ti-microalloying element addition.

Different microstructures of HAZ are derived from the different welding thermal cycles and cooling efficiency. The microstructure of original base metal (BM) on HSLA steels shown in Fig. 5 has demonstrated fine grains of ferrite (F) with some pearlite (P). The application of different mode of welding by TIG torch changes the microstructure of HAZ in welded HSLA steel. The microstructure of HAZ of welded HSLA steel with addition of Ti-microalloying element in Fig. 6 mainly consists of bainite with small fractions of A-F and M-A microconstituents phases. However, the austenite grains are resembled as smaller without any typical columnar shape.

Similar microstructures are reported by [15, 31, and 32]. In this study, the addition of Ti reduced the prior austenite grain size in the HAZ due to the existence of high-volume fraction of TiC and TiN inclusions or intermetallic compound which retarded the austenite grain growth during the welding process. Ti microalloying element acts as nucleation sites for the solidification of the melt pool and the subsequent growth is pinned at the grain boundary. The welded HSLA steel by TIG torch welding technique with the addition of different amounts of titanium to the melt altered the microstructural constituents of HAZ, and different ferrite phases formed including acicular ferrite and Widmanstätten ferrite phases aligned along with the bainitic microstructure and finally enhanced the grain refinement of the morphology. This

morphological characteristic contributes to the improvement of mechanical properties of TIG welded HSLA steel.

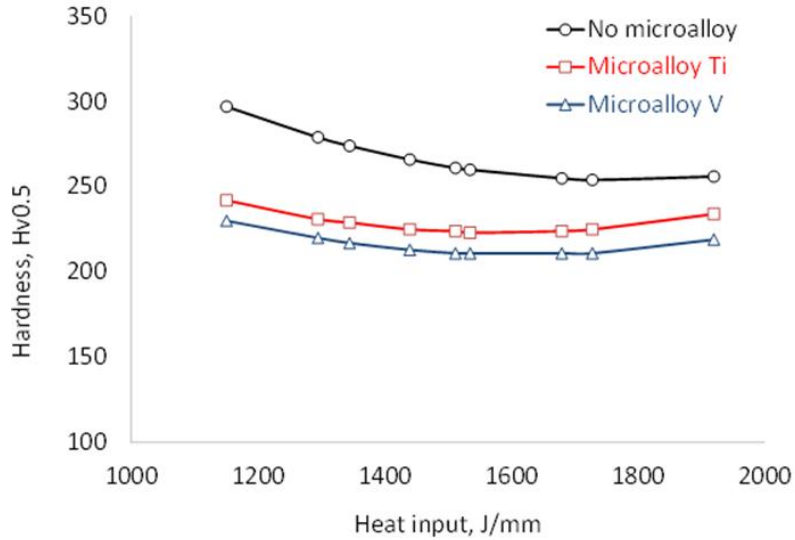


Fig.7: Variation of hardness value for the HAZ with and without microalloying element addition.

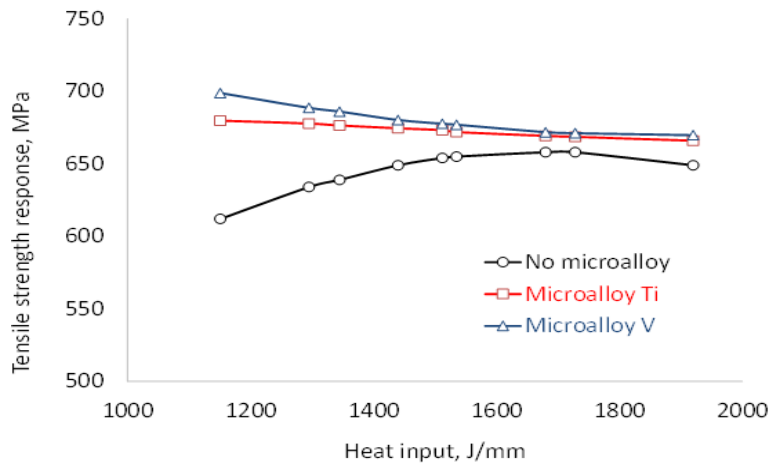


Fig. 8: Variation of tensile strength response on the welding of HSLA steel with and without microalloying element addition.

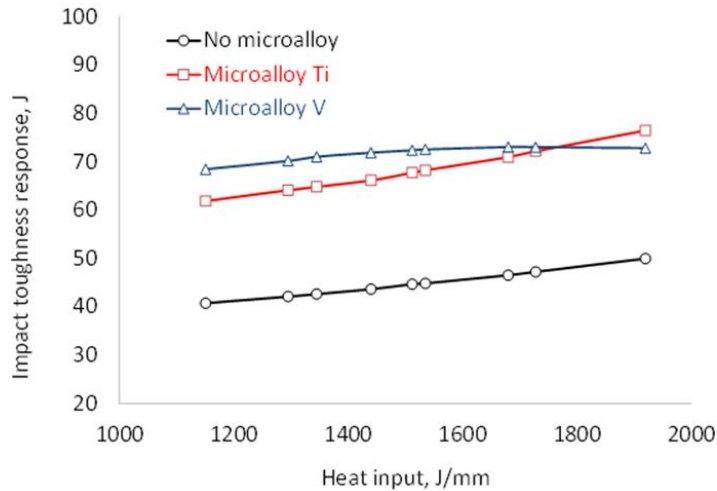


Fig. 9: Variation of impact toughness value on the HAZ with and without microalloying element addition.

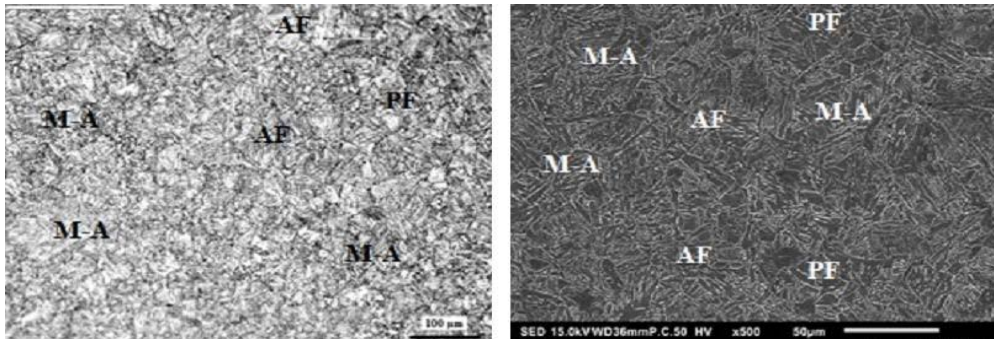


Fig. 10: OM and SEM micrographs of HAZ of welded HSLA steel with 1.0 mg/mm² V-microalloying element addition.

According to literature, the solubility of vanadium in austenite is higher than the other microalloy to form carbide and nitride phase after resolidification of the molten metal. Vanadium carbide, nitride, and carbonitride precipitates have the strong pinning effect on the austenite grain boundaries and on the transformation a fine ferrite grain structure development as well. In the same note, it is believed that small amount of vanadium in structural steels produce a significant refinement in the final ferrite microstructure, through both enhancements of the nucleation of grain boundary ferrite and by intragranular nucleation of ferrite [25, 26]. Fig. 10 shows the HAZ microstructure of melted HSLA steel with 1152 J/mm heat input. It presents the HAZ microstructure of welded HSLA steel with addition of V-microalloying element, mainly consisting of grain boundary polygonal ferrite, with small fractions of A-F and M-A constituents located along the austenite grain boundaries and polygonal ferrite (PF) grain boundaries. However, M-A constituent was also observed along the bainitic-ferrite lath boundaries, which were a common feature in the high strength low alloy steel. This might have a negative effect on the property of the weld since M-A constituents are still present in microstructure and generally reduce HAZ property particularly the toughness and ductility. This finding is similar to the findings reported elsewhere [27, 28].

3.3 Effect of microalloying element addition on mechanical properties

In this section, results are presented on the hardness, tensile strength, and the impact toughness of HAZ of welded HSLA steel without and with the addition of different microalloying elements under different heat inputs as shown in Figs. 7-9. Fig. 7 shows the hardness variation for the HAZ with and without micro-alloying element addition to the welded HSLA steel for different energy input during welding. The HAZ hardness characterization results of welded HSLA steel without microalloying elements revealed that the hardness gradually decreased on increasing the energy input. The addition of alloying elements also affected the hardness. The

reduction of hardness values in the HAZ was approximately 15% for the welded samples with titanium microalloying element addition compared to the welding samples without any additive, while the decrease of HAZ hardness when the vanadium microalloying element was added was approximately 19% compared to the welding samples without microalloying element addition. For all three cases the hardness generally decreased with increasing energy input and was essentially insensitive beyond the energy input of approximately 1680 J/mm . Fig. 8 shows the variation of tensile strength response of the welded HSLA steel with and without micro-alloying element addition for different welding energy inputs.

The tensile strength results of the welded HSLA steel without microalloying elements showed that the ultimate tensile strength increased gradually on increasing the heat input followed by a slight decrease at a higher energy input while there is a remarkable increase in the tensile strength values for all welded HSLA steel samples with the additions of both titanium and vanadium micro-alloying elements compared with welded HSLA steel without microalloying elements. However, there is slight decrease in tensile strength with increasing heat input for both Ti and V additions samples. The reduction in the tensile strength with increasing energy input is assumed to be due to the increased dilution associated with higher energy input which induces dissolution of the grain pinning precipitates resulting in grain coarsening. This trend agrees with the welding metallurgy principle which states that higher heat input results in lowering of mechanical property of weld section [28]. The improvement of ultimate tensile strength values was $\approx 4\%$ for welded samples with Ti additive, while the increase in ultimate tensile strength was $\approx 5\%$ for welded samples with V additive, compared with the welding samples without any addition of microalloying element. Fig. 9 shows the variation of impact toughness value in the HAZ with and without microalloying element addition of welded HSLA steel for different welding heat inputs.

The impact toughness trend of HAZ of welded HSLA steel without microalloying elements and welded HSLA steel samples with the additions of titanium increased gradually on increasing the energy input while there is a marginal increase in the impact toughness values for HAZ of welded HSLA steel with vanadium addition, particularly for heat input above 1510 J/mm . A noticeable improvement in the impact

toughness after the additions of titanium and vanadium microalloying elements was obtained compared to the impact toughness of HAZ for welded HSLA steel without microalloying elements during welding processes. The average increment of impact toughness values in the HAZ was $\approx 30\%$ for welded samples with titanium microalloying element addition while the average improvement of HAZ impact toughness with the vanadium microalloying element addition was approximately 37% compared with the welding samples without the addition of microalloying elements. However, the variation in the impact toughness values with increasing energy input between vanadium and titanium additions was slightly up to approximately 5%.

3.4 Comparison of Ti and V microalloying elements on structure and mechanical performance

Table 5 summarizes a comparison of mechanical performance parameter for Ti-added and V-added HSLA steels after TIG torch melting process whereas, Fig. 11 shows the percentage improvement in hardness, tensile strength, and impact toughness for the same microalloying element additions. The formation of small TiC and TiN particles in the microstructure of high-strength low alloy steel weld metal has been reported by [29] which can be of great strengthening effect and contributes to the improvement of mechanical properties of the current HSLA steel in this investigation. TiS phases significantly influence both the texture and the mechanical properties of HSLA steel. It has been suggested that this compound has an adverse effect on the fracture of welded steels [30]. The formation of these phases (TiN and TiC) plays an important role in the new microstructure development (acicular ferrite) in the nucleation sites for the improvement of mechanical properties. Moreover, titanium carbide and titanium nitride inclusions retard austenite grain growth. The polygonal ferrite also formed during subsequent transformation of austenite to ferrite along the austenite grain boundaries. Consequently, the precipitation of carbides or carbonitrides during cooling cycle of weld pool can prevent the grain growth of austenite. This can be beneficial for refining grains in HAZ and leads to better mechanical properties of welded micro-alloyed high strength steels [30-32]. In one study, it is mentioned that the addition of small amount of Ti revealed an improvement in the high-temperature strength of tantalum alloy [33].

Table 5: Comparison of improved performance properties due to microalloying additions

Performance properties	Hardness, %			Strength, %			Impact toughness, %		
	Ti	V	V - Ti	Ti	V	V - Ti	Ti	V	V - Ti
Heat input, J/mm									
1152	19	23	4	11	14	3	52	68	16
1295	17	21	4	7	9	2	52	67	14
1345	16	21	4	6	7	1	52	67	15
1440	15	20	5	4	5	1	52	65	13
1512	14	19	5	3	4	1	52	62	10
1535	14	19	5	3	3	1	52	62	10
1680	12	17	5	2	2	0	52	57	4
1728	11	17	6	2	2	0	53	55	2
1920	9	14	6	3	3	1	53	46	-7

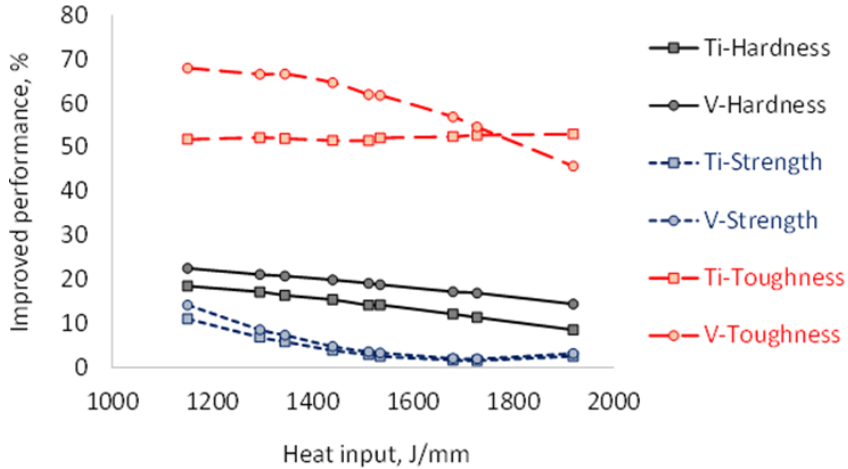


Fig. 11: Comparison of the percentage improvement of the performance properties due to addition of Ti and V microalloying elements.

Vanadium carbide, nitride, and carbonitride particles are known to pin austenite grain boundaries, and on transformation, form a fine ferrite grain structure. There is strong evidence to show that small quantities of vanadium in HSLA steels produce a significant refinement in the final ferrite microstructure (as shown in Fig. 10) through both enhancements of the nucleation of grain boundary ferrite and by intragranular nucleation of ferrite. The presence of vanadium carbide and vanadium nitride enhanced the mechanical properties of welded HSLA steels [33, 34-38]. The XRD results, Fig. 4 demonstrated the characterization of the TIG torch melted microalloying elements (Ti and V) and revealed the existence of new phases in HAZ of HSLA steel containing the intermetallic compound of TiC, TiN, TiS, VC, and VN. The peaks have different concentrations at different angles of the XRD profile which depends on the microalloying element quantities and heat inputs of welding processes [39]. These intermetallic compounds play important roles in the morphology of microstructures and the mechanical properties of HAZ of welded HSLA steel.

In Table 5, mechanical properties performance for Ti-added and V-added HSLA steels after TIG torch melting process are notable which was produced from different heat input of the welding. The addition of both the titanium and the vanadium microalloying elements improved the overall performance properties with a subsequent reduction in hardness and increase in strength and impact toughness. In particular, the microalloying element vanadium demonstrated a greater influence on improving the performance properties. This is illustrated by the difference between V and Ti additions, i.e., “V-Ti” column in Table 5. Compared to titanium the addition of vanadium improved the hardness, the strength, and the toughness by 4%, 3% and 16% respectively corresponding to low heat input of 1152 J/mm. From Fig. 11, the percentage improvement in hardness, tensile strength and impact toughness for Ti and V microalloying element addition is significant. However, the improvement is more prominent at lower heat input and gradually decreases with the increasing heat input. The addition of Ti and V resulted in the improvement of the mechanical performance illustrated by positive values. Overall, the addition of V resulted in a higher performance compared to Ti. The difference in performance between V and Ti is plotted in Fig. 12 which clearly shows the higher performance due to V over Ti. Apart

for the toughness at high heat input corresponding to 1920 J/mm all the points in the graphs are in the positive range.

It was demonstrated that different microstructures were formed with these two microalloying elements, which finally enhanced the grain refinement of the morphology. The morphological characteristic contributes to the improvement of mechanical properties of TIG welded HSLA steel.

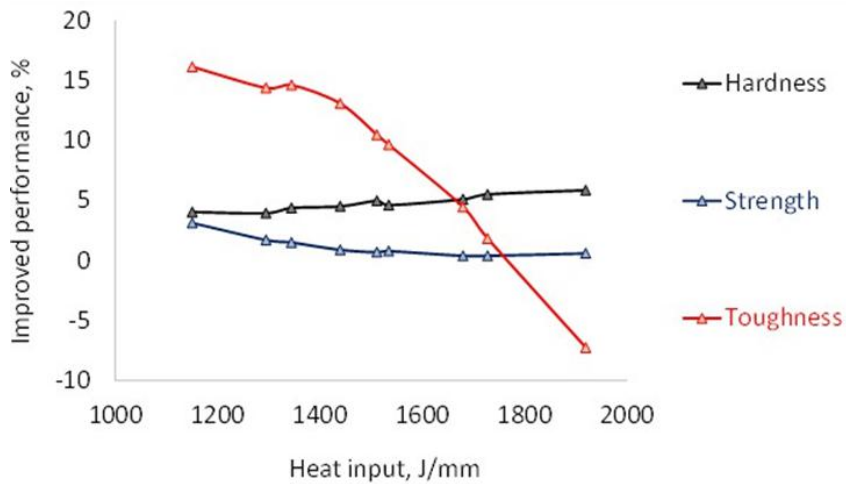


Fig. 12: Percentage difference between the improved performances due to the V microalloying element addition over Ti microalloying element.

4. Conclusions

The present study characterized the microstructure and mechanical properties of HAZ for welded HSLA steel aiming to optimize the microstructure-mechanical property relationship with the addition of Ti and V microalloying elements using TIG torch melting technique. The characteristics of the heat-affected zone (HAZ) were enhanced with a combination of lower hardness, higher strength, and improved impact toughness through the additions of microalloying elements compared to conventional welding without elements. Analysis of results showed that Ti and V microalloying elements significantly influence the HAZ hardness, impact toughness

and the tensile strength of TIG torch melted HSLA steel. A maximum ultimate tensile strength of 692.85 MPa and 729.80 MPa was achieved with Ti and V addition respectively. The reduction in HAZ hardness values of welding samples with the addition of Ti and V addition was approximately 15% and 19% respectively, relative to the welding samples without any microalloying additions. The decrease in HAZ hardness after welding region can reduce the risk of brittle fracture of the welded component.

The average increase in the impact toughness values of the HAZ was approximately 30% for the welded samples with Ti and 37% for welding samples with V compared to the welding samples without the addition of microalloying elements. However, the variation in the impact toughness values with increasing heat input between vanadium and titanium additions was slightly higher, approximately 5%. The overall positive outcome on the mechanical properties of HAZ supports the use of the present technique and encourages further development of a new advanced and sustainable HSLA steel material for a variety of engineering applications.

Acknowledgements

The authors would like to acknowledge the Department of Materials Science & Engineering of faculty of Engineering /Gharyan University for the technical support in carrying out this work, and made this study possible.

References

- [1]Chen, C., Zhao, M.-S., Fung, T.-C., Chiew, S.-P., & Lee, C.-K. (2017). Influence of welding on mechanical properties of high strength steel butt joints. In *Proceeding of Eurosteel 2017* (Vol. 14, pp. 228–235).
- [2]Zhu, P., Li, Y., Chen, B., Ma, X., Zhang, D., & Tang, C. (2018). Research on Microstructure and Properties of Welded Joint of High Strength Steel. *Earth and Environmental Science*, 108, 1–7.
- [3]Muda, W. S. H. W., Nasir, N. S. M., Mamat, S., & Jamian, S. (2015). Effect of Welding Heat Input on Microstructure and Mechanical Properties at Course Grain Heat Affected Zone of ABS Grade A Steel. *ARP Journal of Engineering and Applied Sciences*, 10(20), 9487–9495.

- [4] Nuruddin, I. K. (2012). *Effect of welding thermal cycles on the HAZ microstructure and toughness of multi-pass welded pipeline steels*.
- [5] Rosado, D. B., Waele, W. De, & Vanderschueren, D. (2013). Latest developments in mechanical properties and metallurgical of high strength line pipes. *Sustainable Construction and Design*, 4(1), 1–10.
- [6] Pirinen, M., Martikainen, Y., Ivanov, S. Y., & Karkhin, V. A. (2015). Comparative analysis of the microstructure of the heat-affected zone metal in welding of high-strength steels. *Welding International*, 29(4), 301–305.
- [7] Di, X. J., An, X., Cheng, F. J., Wang, D. P., Guo, X. J., & Xue, Z. K. (2016). Effect of martensite–austenite constituent on toughness of simulated inter-critically reheated coarse-grained heat-affected zone in X70 pipeline steel. *Science and Technology of Welding and Joining*, 21(5), 366–373.
- [8] Hamada, M. (2003). Control of strength and toughness at the heat affected zone. *Journal of the Japan Welding Society*, 4(17), 265–270.
- [9] Xie, H., Du, L. X., Hu, J., Sun, G. S., Wu, H. Y., & Misra, R. D. K. (2015). Effect of thermo-483 mechanical cycling on the microstructure and toughness in the weld CGHAZ of a novel high strength low carbon steel. *Materials Science and Engineering A*, 639, 482–488.
- [10] Aloraier, A., Ibrahim, R., & Thomson, P. (2006). FCAW process to avoid the use of post weld heat treatment. *International Journal of Pressure Vessels and Piping*, 83(5), 394–398.
- [11] Zhao, M. S., Chiew, S. P., & Lee, C. K. (2016). Post weld heat treatment for high strength steel welded connections. *Journal of Constructional Steel Research*, 122, 167–177.
- [12] Musa M. H. A., Md Abdul Maleque, Ali M. Y. (2020), Heat Affected Zone Morphology of TIG Torch Welded HSLA Steel in Presence of Ti and V Microalloying Elements, In book: *Encyclopedia of Renewable and Sustainable Materials*, Vol 4, pp. 439-444, 2020, Elsevier Pub.
- [13] Fletcher, L., Zhu, Z., Marimuthu, M., Zheng, L., Bai, M., Li, H., & Barbaro, F. (2011). Effect of Ti and N concentrations on microstructure and mechanical

- properties of microalloyed high strength line pipe steel welds. *University of Wollongong Research Online*, 1–13.
- [14] Majid, M., & Phanden, R. K. (2015). Effect of TiO₂ Addition in Saw Flux on Mechanical Properties of AISI 1020 Welds Groove face Root opening Root face. *International Journal For Technological Research In Engineering*, 2(7), 1085–1091.
- [15] Rauch, R., Kapl, S., Posch, G., & Radlmayr, K. (2012). High Strength Low Alloy Steel 500 Weldments with Accommodated Qualities to the Base Metal. *BHM Berg- Und Hüttenmännische Monatshefte*, 157(3), 102–107.
- [16] 16. Maduraimuthu, V., Vasantharaja P., Vasudevan M., Bhabani, S. P. (2019). Optimization of A-TIG Welding Process Parameters for P92 (9Cr-0.5Mo-1.8W-VNb) Steel by Using Response Surface Methodology, *Materials Performance and Characterization* 8(4):20180066.
- [17] Anon, Product Catalog, Tianjin Xin'ao Steel Sales Co. Ltd., China, 2021.
- [18] Musa, H. A., Maleque, M. A. and Ali, M. Y. (2018). An Investigation of TIG welding parameters on microhardness and microstructure of heat affected zone of HSLA steel, *IOP Conf. Series: Materials Science and Engineering* 290, 2018, 012041.
- [19] Zhu, Z. X., Kuzmikova, L., Marimuthu, M., Li, H. J., & Barbaro, F. (2013). Role of Ti and N in line pipe steel welds. *Science and Technology of Welding and Joining*, 18(1), 1–10.
- [20] Chengdu Huarui Industrial Co. Ltd., Trading Company,
- [21] Nafisi, S., Arafin, M., Amirkhiz, B. S., Glodowski, R., Collins, L., & Szpunar, J. (2014). Impact of Vanadium Addition on API X100 Steel. *The Iron and Steel Institute of Japan, ISIJ International*, 54(10), 2404–2410.
- [22] Zhu, Z., Han, J., & Li, H. (2015). Effect of alloy design on improving toughness for X70 steel during welding. *Materials and Design*, 88, 1326–1333.
- [23] Gaaz, T. S., Sulong, A. B., Akhtar, M. N., Kadhun, A. A. H., Mohamad, A. B., Al-Amiery, A. A., & McPhee, D. J. (2015). Properties and applications of polyvinyl alcohol, halloysite nanotubes and their nanocomposites. *Molecules*, 20(12), 22833–22847.

- [24] Maleque, M. A., & Adeleke, S. A. (2013). Surface Alloying of CP-Ti Using preplaced Fe-C-Si powder by Tungsten Inert Gas Torch Technique manner. *International Conference on Mechanical, Industrial and Materials Engineering, 2013*, 668–673.
- [25] Mridha, S., Idriss, A. N., Baker, T. N. (2012) Incorporation of TiC Particulates on AISI 4340 525 Low Alloy Steel Surfaces via Tungsten Inert Gas Arc Melting, *Advanced Materials Research.*, Vol. 445, pp. 655–660.
- [26] Han, C., Li, K., Liu, X., Cao, R., & Cai, Z. (2018). Effect of Ti content and martensite–austenite constituents on microstructure and mechanical property. *Science and Technology of Welding and Joining*, 23(5), 410–419.
- [27] Spachinger, S. J., Ernst, W., & Enzinger, N. (2017). Influence of Ti on the toughness of the FGHAZ and the CGHAZ of high-strength microalloyed S700MC steels. *Welding in the World*, 532 61(6), 1117–1131.
- [28] Shi, Y., Sun, K., Cui, S., Zeng, M., Yi, J., Shen, X., & Yi, Y. (2018). Microstructure Evolution and Mechanical Properties of Underwater Dry and Local Dry Cavity Welded Joints of 690 MPa Grade High Strength Steel. *Materials Article*, 11(167).
- [29] Ahmadikhah, R., Sharifitabar, M., & Roudini, G. (2018). Effects of Ti addition on the microstructure and mechanical properties of multi-pass E6010 high-cellulosic electrode weld metal. *Applied Physics A: Materials Science and Processing*, 124:772(11), 1–12.
- [30] Li, L., Song, B., Cheng, J., Yang, Z., & Cai, Z. (2018). Effects of vanadium precipitates on hydrogen trapping efficiency and hydrogen induced cracking resistance in X80 pipeline steel. *International Journal of Hydrogen Energy*, 43(36), 17353–17363.
- [31] Mitchell, P. S. (2005). The Effect of Vanadium on the Microstructure and Toughness of Weld Heat Affected Zones. *Iron and Steel*, 40(V1105-2), 36–42.
- [32] Li, Y., Crowther, D. N., Green, M. J. W., Mitchell, P. S., & Baker, T. N. (2001). The Effect of Vanadium and Niobium on the Properties and Microstructure of

- the Intercritically Reheated Coarse Grained Heat Affected Zone in Low Carbon Microalloyed Steels. *ISIJ International*, 41(1), 46–55.
- [33] Baker, T. N. (2009). Processes, microstructure and properties of vanadium microalloyed steels. *Materials Science and Technology*, 25(9), 1083–1107.
- [34] Lakshminarayanan, A. K., Shanmugam, K., & Balasubramanian, V. (2009). Effect of Autogenous Arc Welding Processes on Tensile and Impact Properties of Ferritic Stainless Steel Joints. *Journal of Iron and Steel Research International*, 16(1), 16, 62-68.
- [35] Beidokhti, B., Kokabi, A. H., & Dolati, A. (2014). A comprehensive study on the microstructure of high strength low alloy pipeline welds. *Journal of Alloys and Compounds*, 597, 142–147.
- [36] Baker, T. N. (2018) Titanium microalloyed steels. *Ironmaking and Steelmaking* . ISSN 1743-2812,
- [37] Aminorroaya-Yamini, S. (2008). *Effect of titanium additions to low carbon , low manganese steels on sulphide precipitation*. University of Wollongong.
- [38] Musa, M. H. A. (2020) Characterization of Heat Affected Zone for TIG Torch Welded High Strength Low Alloy Steel with Microalloying Elements Addition, PhD Thesis, International Islamic University Malaysia.
- [39] Xiangdong Huo, Jinian Xia, Liejun Li, Zhengwu Peng, Songjun Chen, C.-T. P. (2018). A review of research and development on titanium microalloyed high strength steels. *J. Phys. D: Appl. Phys*, 5(6), 1–27.

Multimodal Biometric System Using Dual Digital Watermarking

Abdulmawla Najih^{1,4*}, Salem s.m Khalifa², Salem Enajeh³, Nabila Albannai⁴

^{1,4*}Department of computer engineering, The High Institute of Science & Technology Gharian

²Department of computer engineering College of Science & Technology Alriyayna

³Department of computer engineering, The High Institute of Science & Technology Tripoli

nabdulmawla@gmail.com

المخلص

يعتمد نظام القياسات الحيوية متعدد الوسائط على معرفات بيومترية متعددة لتحديد هوية الشخص الذي أصبح أكثر شيوعاً في المصادقة وتحديد الهوية. نظراً لشعبية النظام متعدد الوسائط، يتم أخذ ثلاثة عوامل (الأمان والمصادقة والمتانة) في الاعتبار عند مصادقة الصورة والتعرف على الوجه وتحديد الهوية البيومترية. يعرض هذا البحث النظام البيومتري متعدد الوسائط من خلال تطبيق نظام العلامة المائية الرقمية المزدوجة. تقوم العلامة المائية المزدوجة المقترحة بدمج علامات مائية عمياء وشبه هشة وقوية في صورة الوجه. لتضمين علامة مائية رقمية عمياء شبه هشة، يُقترح (IWT تحويل الموجات الصحيحة) والإجراء العكسي، وبالنسبة للعلامات المائية الرقمية القوية، يُقترح DCT (تحويل كونتورليت منفصل) و QIM (تعديل مؤشر القياس الكمي). في هذا البحث، تم استخدام اثنين من القياسات الحيوية بما في ذلك الوجه والصوت لنظام القياسات الحيوية. بالنسبة لتضمين العلامة المائية، يتم استخراج الميزات الصوتية لـ MFCC معاملات التردد (Cepstral) وتضمينها في صورة الوجه. يتم تنفيذ عملية اختيار الوجه باستخدام خوارزمية ICP (النقطة التكرارية الأقرب) التي تعمل على أساس أوزان التعلم. يتم اتخاذ القرار النهائي باستخدام التعلم المعزز العميق المسمى "Double Deep-Q Network". يتم استخدام مجموعتين مثل TIMIT (قاعدة بيانات الصوت) و ORL (قاعدة بيانات الوجه) لتقييم النظام واختبار الأداء. يُظهر نظام العلامات المائية المزدوجة المقترح أداءً أفضل من حيث الدقة، ونسبة كفاءة الطاقة EER ، و PSNR ، و SSIM.

Abstract:

Multimodal biometric system relies on multiple biometric identifiers for person identification that becomes more popular in authentication and identification. Due to the popularity of multimodal system, three factors (security, authentication and robustness) are considered for image authentication, face recognition and biometric identification. This paper presents multimodal biometric system by applying double digital watermarking scheme. The proposed dual watermarking is embedding blind semi-fragile and robust watermarks into the facial image. To embed blind semi-fragile digital watermarking, IWT (Integer Wavelet Transform) and Reversible Procedure is proposed and for robust digital watermarks, DCT (Discrete Contourlet Transform) and QIM (Quantization Index Modulation) is proposed. In this, we have used two biometrics including face and voice for biometric system. For watermark embedding, MFCC (Mel Frequency Cepstral Coefficients) voice features are extracted and embedding into facial image. Face selection operation is performed using ICP (Iterative Closest Point) algorithm that works based on learning weights. Final decision making is performed using Deep Reinforcement Learning called “Double Deep-Q-Network”. Two corpuses such as TIMIT (voice) and ORL (Face) are used for system evaluation and performance testing. our proposed double watermarking scheme exhibits better performance in terms of accuracy, EER, PSNR, SSIM,

Keywords: Multimodal, Double watermarking, Face recognition, Discrete Contourlet Transformation (DCT), Quantization Index Modulation (QIM), Integer Wavelet Transform (IWT) and Reversible Procedure.

i. INTRODUCTION

The rapid growth in Information Technology (IT) has revised the need to protect sensitive and personal data from any unauthorized access. Many techniques have been proposed to protect these data, such as the knowledge-based method, where login credentials, such as passwords, Personal Identification Number (PIN) or patterns, are required from the users to access these data. However, the importance of protecting these data and the sensitivity of such methods to simple attacks, such as shoulder

surfing, have imposed the need for more secure techniques [9]. Therefore, many methods have been proposed to protect these techniques from known attacks but the tendency of humans to use easy-to-remember credentials has limited the capabilities of such techniques, as easy-to-remember credentials are also easy-to-predicting [6].

To protect such data, and according to the limited security that Knowledge-based techniques provide, many techniques have been proposed based on biometric information. This information is collected from the user upon authentication and compared to the information of the legitimate users who are allowed to access the system. The user of such information has shown better resistance against attacks that rely on identifying the information used for authentication, as it is more complex to replicate biometric features, than the traditional methods, such as passwords or patterns, in Knowledge-based authentication [10, 13, 16].

One of the widely used techniques to protect the authenticity of information communicated between different parts of the authentication system is digital watermarking, where biometric information is added to the captured biometric image that the biometric features are extracted from. Watermarking techniques are normally used for one of two reasons, which are to prove ownership of the biometric image or to detect any tampering with it. Moreover, some of the watermarking techniques add visible watermarks to the biometric image, while others hide the watermark inside the biometric image, so that, it is not visible unless it is extracted. For tamper detection, hidden watermarks are added to the biometric images, so that, the absence of the watermark or any distortion in the extracted watermark indicates tampering with the original biometric image. Moreover, the watermarking techniques used for tamper detection is fragile, so that, the extracted watermark is highly affected when any attack is executed against the watermarked biometric image [5].

In biometric systems, researchers [4, 14, 15, 17, 18, and 19] have proposed digital watermarking algorithms against geometrical attacks and other attacks. Watermarking is referred to as hidden information and protect against unauthorized persons. To hidden data, certain information is considered and to be embedded on original host image using any water- marking techniques. In this case, original image content could

not affect. Some of the researchers [1, 2, 3, 7, 11, 28, 29, 21, 24, 25, 26, and 27] have proposed frequency domain methods for watermarking while others proposed spatial domain methods [12 and 31]. Recently, researchers have concentrated on double watermarking methods. For each watermarking, they have used separate techniques. Table 1 demonstrates that recently used watermarking techniques. To solve those limitations, in this paper we propose a hybrid double watermarking method to build an online multimodal system by embedding MFCC voice features into face images. The main objective of our multimodal biometric watermarking system is to provide security to biometric data without conceding the quality of both biometric host image and watermark data. The main contributions of our work are as follows:

- DGA-SA (Dynamic Genetic Algorithm with Simulated Annealing). In watermarking, spatial location and best embedding point are required for efficient watermarking. So that DGA- SA is proposed DGA to compute the spatial location of the coefficients and then this suboptimal solution is forwarded to Simulated Annealing for best embedding selection.
- ICP (Iterative Closest Point) for face selection. Face selection is based on the patches. In this face image is split into patches (eye, nose, mouth). In this ICP algorithm the face selection in which closest points selected that will be used for classification.
- Deep Reinforcement Learning algorithm named “Double Deep-Q-Network” which is the recent network, this reduces the complexity and it will be used for face recognition.

The paper is organized as follows: Section 2 is a literature review; Section 3 describes the proposed methodology in three parts; biometric data processing, double digital watermarking and face identification; Section 4 presented database description and experimental results; and Section 5 concludes on the research study carried out.

ii. LITERATURE REVIEW

There is wide collection of approaches have been proposed for watermarking. Almost of them adopt the idea of digital watermarking using transformation methods DWT (Discrete Wavelet Transform), DCT (Discrete Cosine Transform), and DFT

(Discrete Fourier Transform). Some of these transformation methods are briefly reviewed in the following:

The authors of [14] proposed single biometric identifier/unimodal identifier for face recognition using PCA (Principle Component Analysis) and DCT (Discrete Contourlet Transformation). This combined system is used to ensure the image authenticity and security against robust attacks. Experimentation is proved that the system is successful in security, accuracy, robustness and watermarking techniques. The papers [20, 22, and 23] proposed an approach for multimodal biometric authentication system using watermarking technique. Three biometric traits are postulates in this paper are fingerprint, face (physical traits) and signature (behavioral trait). Initially, metamorphose is applied on biometric traits using Discrete Cosine and Discrete Wavelet Transformation. After this watermarking is achieved using singular value decomposition scheme. However, the security of biometric data is preeminent, therefore utmost importance to provide security for individual biometric data. The authors of [3] proposed Phase Congruency Model and DCT for personal identification system. Phase Congruency model is employed the low frequency on DCT coefficients of face image and normalization correlation is based on robust property and human perceptivity. Here authors claims that improve the quality, robustness and recognition accuracy against different types of image processing attacks. The authors of [7] described robust and secure watermarking for biometric data protection. This scheme is proposed for the biometric template protection. Communication channel is used for biometric system and the sparse information of watermark biometric data is generated based on the compressive sensing and wavelet coefficients. The proposed scheme is attaining the best results in accuracy and robustness. The authors of [8] introduced face detection methods for digital image authentication. Biometric watermarking technology is authenticating digital images automatically, in such processing authors proposed face detection methods such as principal component analysis, and eigen feature regularization. The objective of this paper is to find the relationship between the original data and extracted biometric data using neural networks. Authors obtained very promising results in experimentation. The authors of [3] proposed feature based 3-level RDWT [Redundant Discrete Wavelet Transform] for multimodal biometric system. Phase congruency model is used to compute the embedding locations which

preserves the facial features from being watermarked and ensures that the face recognition accuracy. In order to improve the performance of proposed watermarking algorithm, an author uses adaptive user-specific watermarking parameters. 3-level wavelet decomposition of a face image is divided to four subbands such that the size of each subband is equal to the original image, the RDWT redundant space provides additional locations for watermark embedding. To address the issues of 3-level RDWT. The authors of [11] presented multimodal biometric identification system using L-level RDWT decomposition. Two biometric traits of the user i.e. the facial and iris features are embedded independently into the wavelet sub-bands. While using the fused score for evaluation, the accuracy was increased. The robustness of the system has been analyzed against various attacks and the verification accuracy evaluated based on false acceptance rate, area under curve and false rejection rate. The wide range of existing approaches uses single watermarking for authentication and face recognition. Single watermarking does not meet security requirements. To mitigate this, current researchers concentrated on dual/double watermarking [30, 31]. these approaches are not efficient for multimodal biometric system since its aim to satisfy the security requirements. To solve those problems, we designed effective multimodal biometric system which meets those requirements to all extent.

iii. System Overview:

To overcome the aforesaid problems and the best of our knowledge, Double Digital Watermarking for Online Multimodal Biometric System is proposed. The proposed double digital watermarking algorithm is a combination of blind semi fragile and robust watermarks. In blind semi-fragile digital watermarking, Integer Wavelet Transform (IWT) and Reversible procedure is performed. For blind robust digital watermarking, Discrete Contourlet Transform (DCT) and Quantization Index Modulation (QIM) are used. The proposed scheme consists of seven phases: Preprocessing, voice feature (MFCC) extraction, face selection, watermark embedding, extraction, authentication and identification. In first, user face and voice biometric traits are preprocessed like image refinement and normalization. In DCT, image is decomposed with five levels 1, 2, 4,8,16 under the directional band. To identify the best embedding point, we proposed Nature Inspired Algorithms called

DGA-SA (Dynamic Genetic Algorithm with Simulated Annealing). In voice data, Voice information segmented and then MFCC (Mel Frequency Cepstral Coefficients) features extracted and applied for watermark embedding. Before that, face selection is performed using ICP (Iterative Closest Point) Algorithm. In this learning weights computed and less weight will be discarded for online face recognition system. After watermark embedding, information transfer to Multimodal biometric system through communication channel. In this, watermark is extracted using Deep Reinforcement Learning algorithm named “Double Deep-Q-Network”.

This algorithm reduces time and improves the system efficiency. TIMIT and ORL corpuses will be used for evaluating the developed systems. Similarity matching is calculated for each training sample with testing sample and the Euclidean Distance formula is used to calculate the distance between training and testing samples.

A. Preprocessing

The first step of the proposed multimodal biometric system is pre-processing. This process makes the input images better suitable for the subsequent steps. The most important processes such as refinement and normalization are carried out under preprocessing. Also, this process is helpful for the feature extraction. Here, the facial images from the database are refined and normalized. Once the input images are acquired from the database, it undergoes the refinement process after refinement we move to normalization steps in which input image is converting into the range of pixels. In parallel, user voice input can be processed in the system. Voice features are used as a watermark to embed in face image. Segmenting voice sample is a crucial task in recognition. In this we segment voice to embed in the facial image.

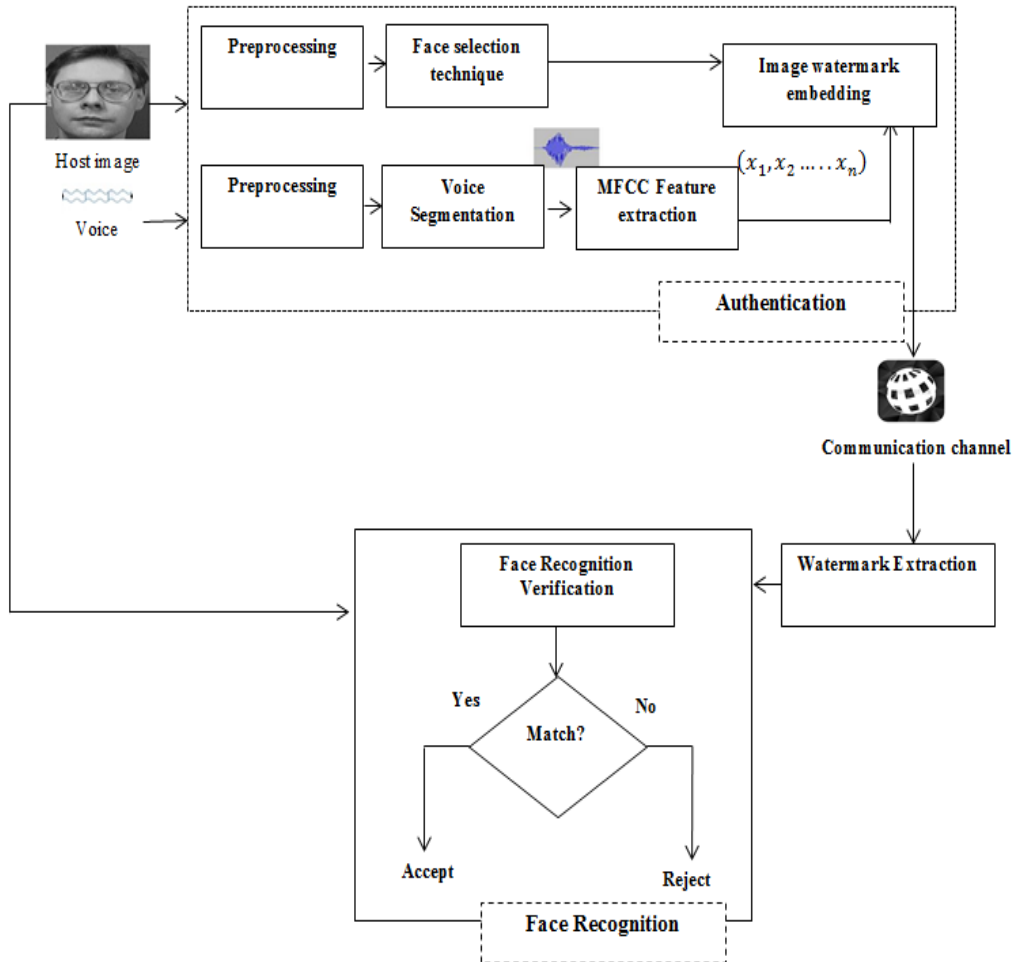


Figure 1: Overall Architecture

B. Voice Feature Extraction:

Voice samples are taken as the input for watermark embedding. Before embedding process, MFCC (Mel Frequency Cepstral Coefficients) features should extract from the voice samples. MFCC is based on cepstral representation and the speech signal spectrum and it is based on auditory processing. Most powerful feature of cepstrum is that repeated patterns or any periodicities. Generally, auditory processing system does not perceive any spectral components in linear scale, but it will perceive spectral components on a nonlinear scale.

The MFCC is defined as the short time power spectrum of a speech signal and the Mel scale wraps the frequency and allows better representation similar to the human auditory system. The Mel scale is defined as the mapping of frequency doubling to a human perception scale. The relation between Mel scale and Hertz scale is

$$f(\text{Mel}) = 2595 \log_{10} \left(1 + \frac{f(\text{Hertz})}{7} \right) \quad (1)$$

MFCC is reduced dimensional form of speech spectrum. In order to compute MFCC, the whole range of audio frequency is divided into frequency bands and also the energy of speech signal with in the band is computed. In MFCC, cepstral coefficients are obtained by computing the log of energy in each band.

C. Face Selection:

In face selection, person face is partitioned into number of patches: eyes, nose, mouth etc. The RGB face color space consists of three additive primary components: Red, Green and Blue. These color components are highly correlated and this will difficult to execute in some image processing algorithms. Many processing techniques are introduced and work on the face partition. In doing so, it produces poor results in all three color spaces. To mitigate this, we proposed Iterative Closest Point Selection algorithm. This algorithm performed with much ease on an image in the RGB Color space.

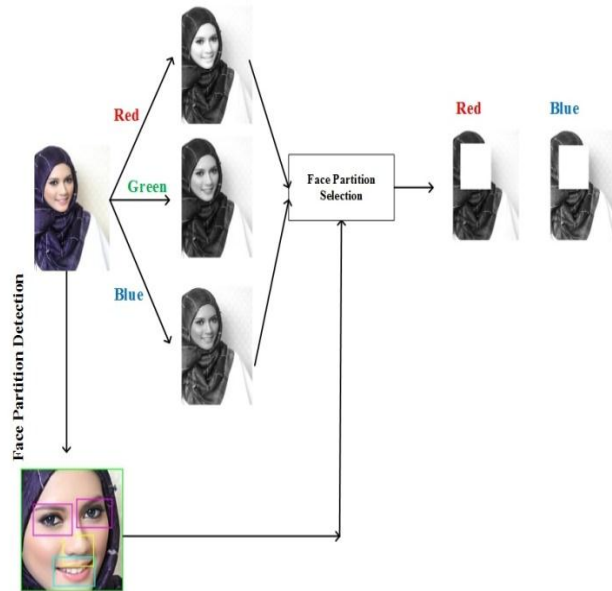


Figure 2: Face selection process

Consider the training samples including N faces (RGB color space). We divide each image into M Overlapping $P \times P$ patches. Each of them by a d -dimensional vector where $d = P^2$. Let i be the certain point and its corresponding closest point j is computed using distance formula. Learning weights (w_{i1}, \dots, w_{ik}) evaluate for the point (i, j) . In this, the points which have the minimum weights have been eliminated in the system.

D. Watermarking

Digital watermarking in multimodal system is defined as the process of embeds biometric data (watermark) into another biometric image. Further, watermark can be detected/extracted to make an assertion of the image. the host image denotes by H , the watermark W , the watermarked image by B and the extracted watermark w' , N can be considered as attacks or noise and the $E(H, W)$ and $D(C)$ be the embedding and extracting function respectively.

the spatial location is computed by the following equation

$$I(a(r, \theta), b(r, \theta)) \rightarrow I(r, \theta) \quad (2)$$

Where I represent the image, $a(r, \theta), b(r, \theta)$ are the coordinates of a, b of the original image and r is the radius lies on the interval $[0, 1]$ and θ is angle between $[0, 2\pi]$.

double watermarking is proposed using hybrid approaches. Here fragile watermarking for tampering detection and robust watermarking for transmitting the MFCC features to the system. The embedding and extraction of watermarking are briefly described in the following sections.

- **Nature Inspired Algorithms (DGA with SA):**

Searching best embedding co-efficient in image is a quite challenging and essential task. Nature inspired evolutionary searching algorithms introduced to select the best embedding point. In this scheme, we proposed Dynamic Genetic with Simulated Annealing for watermark embedding. As a result of this, the capacity is minimized by embedding the selected co-efficient. Dynamic Genetic Algorithm is an evolutionary based searching method approach that consists of natural genetics to solve the global optimization problems. Natural genetics are using operators such as mutation, crossover and selection for optimization. Chromosomes represent the candidate solutions with assigned the score to each of them. By applying genetic operators to chromosomes, we get the new offspring. After the generations of new offspring, chromosomes have better score values that considered being a sub-optimal solution. After applying DGA, SA is started. Simulated Annealing is another evolutionary based search method to find the best solutions. In mathematical side, SA initiated from the starting point and followed by next new candidate solutions is randomly generated. At this point, SA has taken long computational time. To avoid such issues, we combined Dynamic Genetic Algorithm and Simulated Annealing. At the starting point, parameters are initialized such as population size, number of variables, lower crossover and mutation rates, lower and upper bounds for each variable, annealing, selection method and temperature functions are defined. Then starts GA algorithm and stopping criteria are defined as a certain number of generations. At the end of this

Genetic algorithm, sub-optimal solution is generated and then SA is employed with the initial solution from the first part of the algorithm. Flowchart of the DG with Simulated Annealing is illustrated below.

Algorithm for Dynamic Genetic with Simulated Annealing

//Dynamic Genetic Algorithm

Step 1: Initialize the parameters N (population size)

Step 2: Evaluate the chromosomes

Step 3: Select the best chromosomes

Step 4: Repeat //Adaptive Determination of genetic parameters

1. Determine P_c (Crossover Probability) and P_m (Mutation probability), and
2. Perform crossover and mutation
3. Evaluate the chromosomes

Step 5: If average fitness of population is above the fitness average //user defined threshold (T)

{Return the solutions
} Else

Mutate top e solutions in the current population

4. Iterate the step 2 through 5

Output: Sub-optimal solution

//Simulated Annealing

Step 1: Parameters initialization: Initial solution S, Iterations $K=1 \dots L$ of each T, and Initial Temperature T

Step 2: Update T for each iterations

Step 3: Calculate the increment $\Delta E = E(S') - E(S)$ where E(S) is the evaluation function

Step 4: Criterion for Metropolis: If ΔE is greater than 0 then accept S' as the new solution otherwise S' as the new solution with the acceptable probability $P(e^{\Delta E} / T)$

Step 5: If the termination condition is satisfied, the current optimal solution as the output. After that, terminate the program.

Output: Optimal solution (F^{Best})

• **Blind Semi-fragile watermarking**

Blind semi-fragile watermarking can be performed using Integer Wavelet Transform and it can be invisible for users. It has a shift invariant behavior and the errors of reconstruction will decrease after embedding in cover image. As a results of the robustness of the watermarking method will increase.

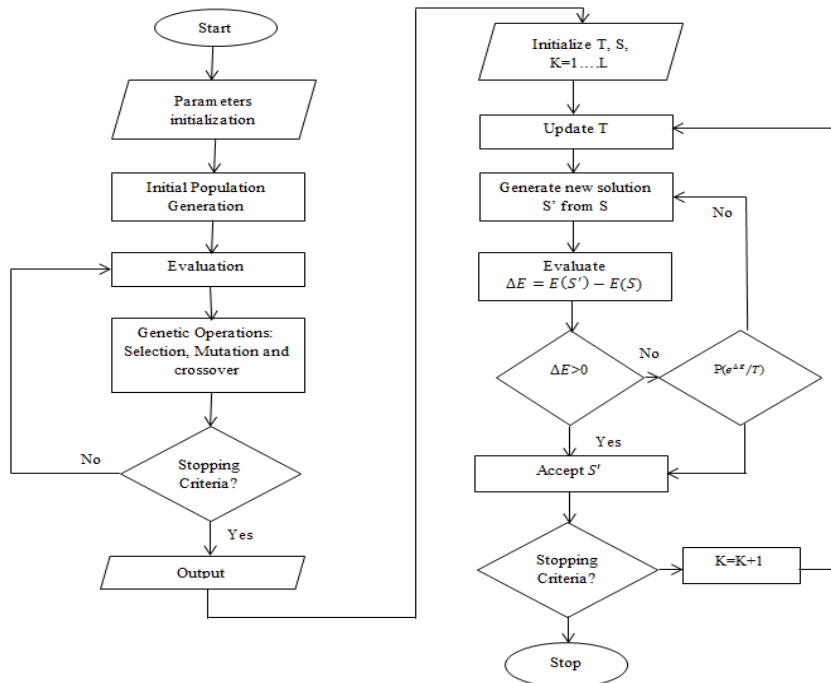


Figure 3: Flowchart for DGA with SA

Algorithm: IWT based blind semi-fragile watermark embedding algorithm

Input: Host image and MFCC features (x_1, x_2, \dots, x_n)

Output: Watermarked image

Begin

Read the image and convert it to gray scale

Decompose the image using IWT

Using the 5th bit, choose the subbands

Compress 5th bit data using arithmetic coding

Compressed data insertion and the watermark features into the host image

Compute IIWT (Inverse-IWT) to get the watermarked image

End.

- **Robust Watermarking**

For robust watermarking, we select discrete contourlet transformation for watermark embedding because it captures the directional edges and smooth contours from the image and its better than the other conventional transforms namely DWT, DCT and DFT. Human Visual system is less sensitive to the image edges and watermarking is applied on the contourlet domain, which denotes image edges. It improved robustness due to selecting the embedding point using algorithm () and optimum control of its quantization scalar factor. However, the perceptibility of the watermarked image degrades. In our scheme, QIM (Quantized Index Modulation) is applied all sub bands when we reconstruct the watermarked image. Because the novel arrangements of the subbands preserve the robustness, so the proposed scheme is highly robust against various low-frequency attacks.

- **Discrete Contourlet Transform:**

Discrete Contourlet Transformation is a new enhanced image decomposition method to embed the watermark effectively. It outperforms than the DWT, RDWT

and DCT. Contourlet transformation is categorized into two phases: LP (Laplacian Pyramid) decomposition and DFB (Directional Filter Banks). In DCT, the number of directional subbands at each level is set to 2^n where n is a positive integer number where $n=1, 2, 3, 4, 5$ then we get the 1, 2, 4, 8, 16 subbands as shown in figure 4. The Energy of subband $S(i, j)$ is computed by the following expressions:

$$E = \sum_i \sum_j |S(i, j)|^2 \quad (3)$$

- **Quantization Index Modulation:**

QIM is a class of embedding methods, termed the quantization index modulation technique. It achieves efficient tradeoffs among information-embedding capacity and robustness of embedding. A particular quantizer is chosen from a set of possible quantizers by using watermark information as an index and then applied to the host information to embed the watermark. Assume that one bit $s \in \{0, 1\}$ is to be embedded and m denotes the host signal. Two quantizers will be considered and generated $Q_i(m)$, where $i=0, 1$. Watermark bit identifies the selection of the quantizer $Q_i(m)$ with a step size Δ , which can be computed as follows:

$$Q_i(m) = Q(m - d_i) + d_i, \quad i=0, 1$$

Where $Q(m) = \Delta \times \text{Round}(m/\Delta)$,

$d_0 = -\Delta/4$ and $d_1 = \Delta/4$ round (num) rounds num to the nearest integer.

$$Q_i(m') \in (Q_0, Q_1)$$

The watermarked signal value m' computed using two quantizers (Q_0) and (Q_1) using the following expression:

$$m' = \begin{cases} Q_0(m), & s = 0 \\ Q_1(m), & s = 1 \end{cases}$$

In the watermark extraction process, the S' can be extracted from the signal of m' by resolving the optimization problem.

$$S' = \arg \min_{s \in \{0,1\}} \|m'' - Q_S(m'')\| \quad (4)$$

- **Watermark Embedding:**

In the proposed scheme, the watermark embedding can be formulated in the following process:

Step 1: The host image H is transformed into the contourlet domain. The lowpass subbands of the coefficients of the host image are selected to embed the watermark. $H_{S,D}(i,j)$ is the host image contourlet coefficients where S is the resolution scale and D is the frequency direction. We embed the watermark in the best embedding point because best embedding point is improving the performance of security.

Step 2: Apply QIM on each subbands of the host image.

Step 3: Use quantizers to produce watermark embed information for both bits 0 and 1.

Step 4: Before embed the watermark, strength of the watermark embedding (α) is derived from the visibility function. It is expressed by:

$$VF = \frac{1}{1 + \sigma_1^2(a, b)} \quad (5)$$

Where $\sigma_1^2(a, b)$ is embedding regions local variance and for every local embedding region, the watermark embedding strength is adaptively modulated. Then the adaptive embedding strength is derived from the following strength

$$\alpha = (1 - NF) \cdot \beta \quad (6)$$

Where β is represents the predefined embedding strength for local watermark regions.

Step 5: After that, MFCC features sequence (x_1, x_2, \dots, x_n) to the number of best selected contourlet coefficients points using the following function:

$$H'_{S,D}(i, j) = \begin{cases} \frac{W \cdot \alpha}{F^{Best}(i, j)} \cdot H_{S,D}(i, j), & F^{Best}(i, j) \neq 0 \\ H_{S,D}(i, j), & F^{Best}(i, j) = 0 \end{cases} \quad (7)$$

Where $H'_{S,D}(i, j)$ and $H_{S,D}(i, j)$ denotes original and watermarked coefficients respectively. $F^{Best}(i, j)$ is the best embedding point of the host image H.

Step 6: Apply IDCT on the modified QIM contourlet coefficients to obtain the watermarked image.

Step 7: Obtain the watermarked image H'

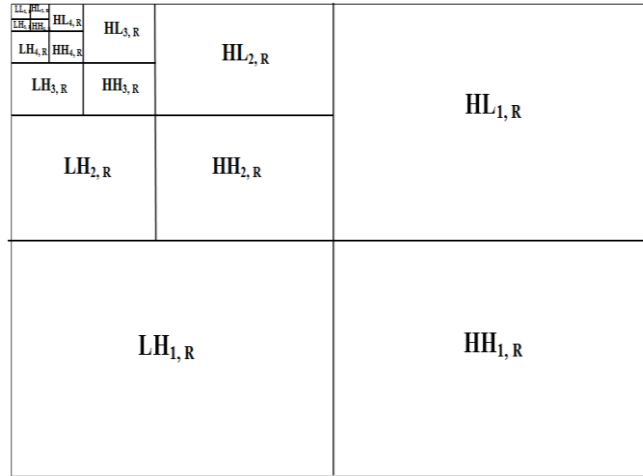


Figure 4: DCT Decomposition with 5-levels

Algorithm: DCT with QIM based Robust Watermark embedding algorithm

Input: Host image, MFCC features (x_1, x_2, \dots, x_n) and F^{Best}

Output: watermark image

Begin

Read the watermark image and apply DCT

Decompose the image into 5-levels $\{LL_{1,R}, \dots, LL_{5,R}\}, \{HL_{1,R}, \dots, HL_{5,R}\}$
 $\{HH_{1,R}, \dots, HH_{5,R}\}, \{LH_{1,R}, \dots, LH_{5,R}\}$ using DCT

Choose lowpass subbands from the decompose image

F^{Best} is selected using DGA-SA

Apply QIM on each subbands

Inserting (x_1, x_2, \dots, x_n) into watermark image

Arrange Quantize levels

Compute IDCT (Inverse-DCT) to get the watermarked image

End

- **Watermark Extraction:**

The steps of watermark extraction process are the same steps of the process of watermark embedding. Watermark extraction are performed as follows: First, detect the voice segments in watermarked signal and then extract the watermark information from the embedding locations depending on the best embedding locations that generated using DG with SA as in the watermark embedding.

- **E. Face Recognition:**

The process of face recognition is carried out by using Double-Deep-Q-Network. Consider the classification in multimodal biometric decision. Suppose we have N learning samples $\{a\}_{i=1}^N \in R^l$ and corresponding class labels $b_i \in \{0, 1\}$ where 0 represents an impostor and 1 represents genuine person. Double Deep-Q-Network is the reinforcement algorithm that newly created in neural networks. The major advantage of this algorithm is to generalize learning across actions without changing of reinforcement algorithm. Value functions are considered here. First we can describe about Deep-Q Network. There are two key aspects of networks are considered that are model free in sense by the environment and experience replay. The network parameters are $Q(m, x, \theta)$ with parameters of θ . To evaluate this network, loss functions must be optimized for n iterations.

$$L_n(\theta_n) = E_{m, x, r, m'} \left[\left(y_n^{DQN} - Q(m, x, \theta_n) \right)^2 \right] \quad (8)$$

Where $y_n^{DQN} = r + \gamma \max_{x'} Q(m', x', \bar{\theta})$

Where $\bar{\theta}$ denotes the parameters of a separate and fixed target network. In online, we use the Q-Learning for the network parameters $Q(m, x, \theta_n)$. Specific gradient is used to update the parameters of network.

$$\nabla_{\theta_n} L_n(\theta_n) = E_{m, x, r, m'} \left[\left(y_n^{DQN} - Q(m, x, \theta_n) \right) \nabla_{\theta_n} Q(m, x, \theta_n) \right] \quad (9)$$

In learning, database D of experiences (m_t, x_t, r_t, m_{t+1}) from many occurrences. During training, the current experience is prescribed from D uniformly at random manner.

$$L_n(\theta_n) = E_{m, x, r, m'} \cdot u(D) \left[\left(y_n^{DQN} - Q(m, x, \theta_n) \right)^2 \right] \quad (10)$$

In DQN Q-learning algorithm, select and evaluate action gives the same values while max operator uses these same values for solving optimization problem. This will lead to the overoptimistic problem. To overcome this, Double Deep-Q-Network is proposed

$$y_n^{DQN} = r + \gamma Q(m', \arg \max_{x'} Q(m', x', \theta_n); \bar{\theta}) \quad (11)$$

F. Euclidean Distance Measure:

To evaluate the similarity or the dissimilarity between the two images, Euclidean Distance is used.

Similarity matching for Face ($S_{v(i,j)}$):

$$S_{f(i,j)} = 1 - d(u_i, v_j) \quad (12)$$

Where u_i training samples and v_j is the testing sample and $d(u_i, v_j)$ is the Euclidean Distance between the training and testing sample and it is evaluated by the following expression:

$$d(u_i, v_j) = \sqrt{\sum_{z=1}^M |u_z - v_z|} \quad (13)$$

Where M is the total number of samples in database and u_z, v_z is the training and testing samples.

Similarity Matching for Voice ($S_{v(i,j)}$):

$$S_{v(i,j)} = 1 - d(u_i, v_j) \quad (14)$$

Where u_i training samples and v_j is the testing sample and $d(u_i, v_j)$ is the Euclidean Distance between the training and testing sample and it is evaluated by the following expression:

$$d(u_i, v_j) = \sqrt{\sum_{z=1}^R |u_z - v_z|} \quad (15)$$

Where R is the total number of samples in database and u_z, v_z is the training and testing samples.

G. Score Fusion Method:

In our proposed system, score fusion method is carried out to combine each biometric score since this method is easy to access and combine the scores of different biometric modalities. Fusion at match score level uses sum method. Let $S: \mathbb{R}^1 \rightarrow \mathbb{R}$ is the hypothesis function mapping these pattern features onto a scalar measure for decision inference. $Fusion_{score}$ produces a continuous output then the output must be threshold in order to label each sample as *genuine_{user}* or Impostor-User. Given a decision threshold τ , and τ between the $[0, 1, \dots, 9]$. Now the fusion score is expressed as,

$$F_{S(i,j)} = S_f(i,j) + S_v(i,j) \quad (16)$$

$$Fusion_{Score} = \begin{cases} 1 (= genuine_{user}) & \text{if } F_s(i, j) \geq \tau \\ 0 (= impostor_{user}) & \text{if } F_s(i, j) < \tau \end{cases}$$

iv. EXPERIMENTAL RESULTS

This section describes the experimental results and the performance of the proposed system.

A. Experimental Setup

For our implementation, we used Matlab. The performance of the proposed multimodal biometric watermarking system has been tested upon ORL and TIMIT databases. Whenever an ownership claim is to be resolved, the face features and voice features are extracted from the suspected watermarked image and compared with the other training samples of the user stored in the two databases. If a match is found from the database, it is categorized as genuine otherwise it taken as impostor attempt. The most important performance factor for the success of any biometric system (uni/multimodal) is its recognition accuracy. In order to validate and verify the proposed system, various factors are considered and tested. The multimodal biometric traits have been described and tested in detail as follows:

B. Databases Description:

For the experimental studies, the multimodal biometric data of ORL and TIMIT databases are taken. ORL contains 40 distinct subjects with the size of 92×112 pixels and 256 grey levels per pixel. Some of the images are taken at different facial expressions like smiling, not smiling, closed eyes, open eyes, anger, etc. The entire facial images were taken at a dark homogenous background with the subjects in some side movements (upright, downright and frontal position). TIMIT corpus consists of speech data for the 630 subjects of 8 dialects, 6300 utterances and 10 sentences in American English. The corpus contains totally 5 hours of speech. All 630 speakers are native speakers of the United States. In addition, auxiliary subjects were recorded but are not considered in the CD-ROM.

C. Parameters Description:

The performance of the system is generally based on the evaluating imperceptibility, robustness and security measures like PSNR, SSIM, EER and other metrics. But when it comes to a multimodal biometric watermarking system, we need to ensure the performance in terms of accuracy. A watermarked system should further

enhance the security aspects of the biometric traits such as face and voice used without compromising in its quality and features. For the proposed algorithm, we have verified the performance based on with watermarking and without watermarking using face, voice and multimodal in terms of accuracy, equal error rate (ERR), PSNR and SSIM. The details are described as follows:

Peak Signal to Noise Ratio (PSNR): PSNR is widely used and accepted measure of the fidelity of the watermarking method and allows visual inspection between original images and watermarked or reconstructed images. It is evaluated by the following expression.

$$PSNR = 10 \log_{10} \frac{255^2}{MSE} \quad (17)$$

Where $MSE = \frac{\sum_{i=1}^m \sum_{j=1}^m (f(i,j) - f'(i,j))^2}{m \times n}$ where f and f' are the two images being compared.

Structural Similarity Index (SSIM): It is a similarity measure between two images of which one image is considered as of perfect quality where $SSIM(x,y)$ is given as follows;

$$SSIM(x,y) = [f(x,y)]^\alpha * [c(x,y)]^\beta * [s(x,y)]^\gamma \quad (18)$$

Equal Error Rate (EER): is also known as crossover rate/crossover error rate. The EER is used to evaluate the performance of our proposed multimodal biometric system. It is used find the value of threshold for FAR (False Accept Rate) and FRR (False Recognition Rate). The lower EER value indicates the better performance and also it improves the accuracy.

$$Equal\ Error\ Rate = \frac{False\ Accept\ Rate}{False\ Recognition\ Rate} \quad (19)$$

Recognition Rate (RR): is also referred as accuracy. RR is the percentage of detected images from the total number of images.

$$\text{Recognition Rate} = \frac{\text{No.of corrected identified images}}{\text{Total no.of images}} * 100 \quad (20)$$

D. Comparative analysis:

The comparative analysis of the proposed method with existing mechanisms is carried out using the EER, PSNR, accuracy and SSIM. The results of the existing mechanisms are taken from the existing techniques [15, and 11]. Here multimodal biometric techniques have been compared using various performance metrics. From Table 1, we understand that our proposed techniques showed the higher performance in terms of accuracy, PSNR, EER and SSIM.

Table.1 presents various multimodal methods based on digital watermarking techniques. As seen almost of the multimodal approaches have been applied face and voice metrics for biometric system as well all of the systems have some pros and cons. From the table, we have analyzed there were not strong and robust watermarking technique which can provide security, robustness, imperceptibility, capacity and memory criteria. On the other hand, watermark embedding effect is degrading the performance of the face recognition system

TABLE1. Comparison of Different Watermarking Techniques

Techniques	Merits	Limitations
LSB	<ol style="list-style-type: none">1. Easy to use and understand2. High perceptual transparency3. Image quality low degradation	<ol style="list-style-type: none">1. lack of basic robustness2. Cropping and scaling vulnerabilities3. Noise vulnerability

DCT	<ol style="list-style-type: none"> 1. In digital watermarking, the watermark is embedded into the coefficients of the middle frequency. So the image visibility will not be affected 2. Does not affect pixels themselves with each other 3. High robustness 	<ol style="list-style-type: none"> 1. Lack of invariance (block wise DCT destroys invariance) 2. Higher frequency
DWT	<ol style="list-style-type: none"> 1. Good in localization 2. Higher compression ratio 	<ol style="list-style-type: none"> 1. Computation cost is high 2. High compression time 3. Blur/noise edges of images
RDWT	<ol style="list-style-type: none"> 1. Invariance property achieved translation 2. Sufficient embedding capacity 	<ol style="list-style-type: none"> 1. Lack of spatial location 2. Best watermark embedding is required in L-Level decomposition.

Two image quality assessment metrics such as Peak Signal to Noise Ratio (PSNR) and Structural Similarity Matrix have been measured to test the performance of imperceptibility of the double watermarking mechanism. Both IQA metrics are well-known conventional metrics for pixel based image operation. From the table 2, we proved that our proposed system achieves good performance in both IQA metrics and also it improves the imperceptibility. Generally, SSIM lies between 0-1. Note that the higher IQA value always implies higher visual quality of the original watermarked image.

TABLE 2. Comparisons of the functionalities of our double watermarking method and related double watermarking mechanism

	Existing	Proposed Approach
Dual watermarks	Fragile + Robust	Fragile + Robust
Embedding domain	Spatial domain + DWT	DCT+QIM
Visibility	Invisible + Invisible	Invisible + Invisible
Blind Extraction	Yes + Yes	Yes +Yes
Target image	Color (RGB)	Color (RGB) and voice
PSNR dB	~ 40dB (40.32)	~ 48dB (48.9835)
Copyright Protection	Yes	Yes
Image Authentication	Yes	Yes
Average Recognition Rate (%)	99.97%	99.98
Robustness	No	Yes
Security	Yes	Yes
SSIM	0.9830	0.9879

TABLE3. Results for our Multimodal Biometric System

	EER (%)			Recognition Rate (%)
	Voice	Face	Multimodal	
Without watermarking	7.5714	8.25	4.25	97.90
with watermarking	7.5714	7.2574	3.333	99.98

TABLE4. Results for Existing Multimodal Biometric System

Mechanism	Recognition Rate (%)		
	Voice	Face	Multimodal
Without watermarking	86.8	89.4	94.0
with watermarking	86.8	89.4	94.0

To further demonstrate the system performance, we compared the proposed system recognition rate with existing system [29]. The comparison results of proposed and existing systems are shown in table 3 and 4. In table 3, the recognition rate of our proposed system is 99.98% which is better than the existing system.

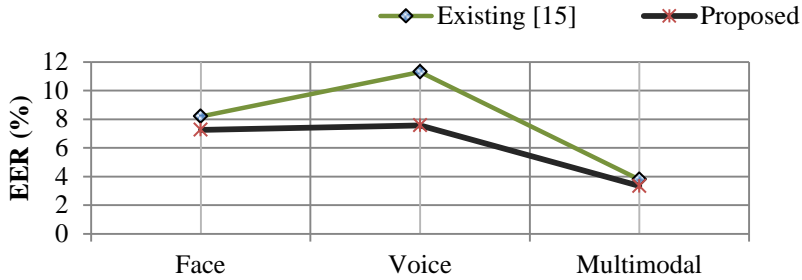


Figure 5: Results of EER

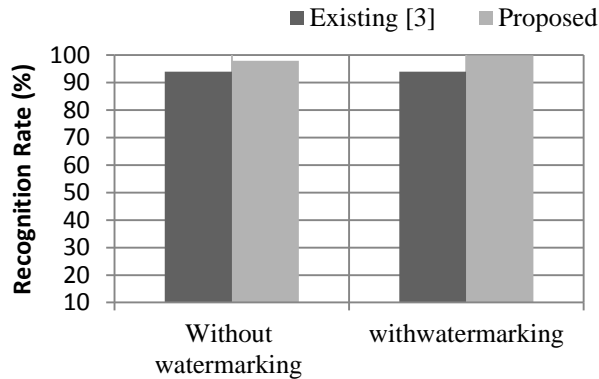


Figure 6: Results of Recognition Rate

v. CONCLUSION

In this paper, we have proposed a blind double digital watermarking method with multimodal biometric system to improve the previous works in area of spatial and temporal domain in terms of robustness, security, authentication and imperceptibility. An important aspect of the proposed digital image watermarking system has the development of watermarking for authentication and recognition. The developed dual watermarking is comprised with blind semi-fragile and robust watermarks into the facial image. Face selection process is proposed to preserve most of the discriminative

features of face image and to secure face image by applying image watermarking process. This face selection process is not only enhancing the performance of face recognition system, but also improving the process of feature extraction. Double Deep-Q-Network is performed for face recognition process which reduces the complexity and improves the accuracy of recognition process. After completion of recognition process, score fusion method is expressed to identify the genuine or imposter user. our proposed double watermarking scheme exhibits better performance in terms of accuracy, EER, PSNR, SSIM,

REFERENCES

- [1] Wadood Abdul, “Securing Biometric Authentication through Multimodal Watermarking”, 3rd International Conference on Artificial Intelligence, Modeling, and Simulation, 2015
- [2] Bairagi Nath Behera, V.K.Govindan, “Improved Multimodal Biometric Watermarking in Authentication Systems Based on DCT and Phase Congruency Model”, International Journal of Computer Science and Network, Vol.2, Issue. 3 and 2013
- [3] Mayank Vatsa, Richa Singh, Afzel Noore, “Feature based RDWT watermarking for multimodal biometric system”, Image and vision computing, 2007.
- [4] A. Lathika, D. Devaraj, “Artificial Neural Network based Multimodal Biometrics Recognition System”, International Conference on Control, Instrumentation, Communication and Computational Technologies, 2014
- [5] Piotr Stefan Nowak, Wojciench Sankowski, Pawel Krotewicz, “3D Face and Hand Scans Acquisition System”, 23rd International Conference on Mixed Design of Integrated Circuits and Systems”, 2016
- [6] Tudor Barbu, Adrian Ciobanu, Mihaela Luca, “Multimodal Biometric Authentication based on Voice, Face and Iris”, The 5th IEEE International Conference on E-Health and Bioengineering, 2015
- [7] Rohit M. Thanki, Ved Vyas Dwivedi, and Komal R.Borisagar, “Robust and Secure Watermarking using Sparse Information of watermark for Biometric data protection”, NIRMA University Journal of Engineering and Technology, 2016.
- [8] Wioletta Wojtowicz and Marek R.Ogiela, “Biometric watermarks based on face recognition methods for authentication of digital images”, Security and Communication Networks, 2014

- [9] Abdulmawla Najih, S.A.R. Al-Haddad, Abd Rahman Ramli, S.J. Hashim, Mohammad Ali nematollahi, “Digital image watermarking based on angle quantization in Discrete Contourlet Transform”, Journal of Kind Saud University-Computer and Information Sciences, 2016.
- [10] Rohit M. Thanki, Komal R. Borisagar, “Novel Approach for Multimodal Biometric System using Compressive Sensing Theory based Watermarking”, International Journal of Computer Science Engineering, Vol. 3, Issue. 4, 81-90, 2013
- [11] Priyanka Singh, Balasubramanian Raman, Partha Pratim Roy, “A multimodal biometric watermarking system for digital images in Redundant Discrete Wavelet Transform”, Multimedia Tools and Applications, Springer, 2016
- [12] Amit Kumar Singh, Nomit Sharma, Mayank Dave, Anand Mohan, “A Novel Technique for Digital Image Watermarking in Spatial Domain”, 2nd IEEE International Conference on Parallel, Distributed and Grid Computing, 2012
- [13] Mohd Rizal Mohd Isa, Salem Aljaresh, Zaharin Yusoff, “A Watermarking technique
- [14] to improve the security level in Face Recognition Systems”, 2016
- [15] [14]. Su wang, Roland Hu, Huimin Yu, Xia Zheng, R.I. Damper, “Augmenting Remote Multimodal Person Verification by Embedding Voice Characteristics into face images”, IEEE international conference on multimedia and expo workshops, 2013.
- [16] Methaq talib Gaata and Refan Aamer Jafer, “Adaptive Watermarking Technique for Speech Signal Authentication”, International Journal of Computer Science and Information Technology, Vol.8, No.4, 2016
- [17] Hashim, R. R. S. J., & Albannai, N. Matching Fingerprint Images for Biometric Authentication using Convolutional Neural Networks. [17]. Ala,E,O (2017). Joint MFCC-and-Vector Quantization based Text-Independent Speaker Recognition System. IEEE International Conference on Communication, Control, Computing and Electronics Engineering.
- [18] Shashi Choudary and Naveen Choudhary, “Intensifying the Security of Multimodal Biometric Authentication System using Watermarking”, Global Journal of Computer Science and Technology, Vol. 15, Issue. 4 and 2015
- [19] Ibrahim A. El rube, Mohammed Abou El Nasr, Mostafa M. Naim, Mahoud Farouk, “Contourlet versus Wavelet Transform for a Robust Digital Watermarking technique”, International journal of electrical, computer energetic, electronic and communication engineering, Vol. 3, No.12, 2009.

- [20] Bali,M (2013).Face Recognition using Eigen Faces and Transmission of Hidden Data using Watermarking Authentication. International Journal of Engineering and Computer Science.2(6), 1827-1833.
- [21] Sirvan Khalighi, Parisa Tirdad, and Hamid R. Rabiee, “A Contourlet based Image Watermarking Scheme with High Resistance to removal and geometrical attacks”, EURASIP Journal on Advances in Signal Processing, 2010
- [22] Amit Mehto, Neelesh Mehra, “Adaptive Lossless Medical Image Watermarking Algorithm based on DCT and DWT”, International conference on Information Security and Privacy, 2015
- [23] Yuqiang Cao, Weiguo Gong, Mingwu Cao, SenBai, “Robust Biometric Watermarking Based on Controulet Transform for Fingerprint and Face Protection”, International Symposium on Intelligent Signal Processing and Communications systems, 2010.
- [24] Yahya AL-Nabhani, Hamid A. Jalab, Ainuddin Rafidah Md Noor, “Robust watermarking algorithm for digital images using discrete wavelet and probabilisticneural network”, Journal of Kind Saud University-Computer and Information Sciences, 27, 393-401, 2015
- [25] BinMa., Yunhong, W., Chunlei, L., Zhaoxiang, Z., & Di, H. (2014). Secure multimodal biometric authentication with wavelet quantization based fingerprint watermarking. Springer Multimedia Tools and Applications, 72(1), 637-666.
- [26] Mohd,R,M,I., Salem,A,Z,Y (2016). A Watermarking technique to improve the security level in Face Recognition Systems.
- [27] Gil-Je Lee-Kee-Young Yoo, “An improved double image digital watermarking scheme using the position property”, Multimedia Tools and Applications, Springer, 2014
- [28] Vandana S Inamdar, and Priti P Rege, “Dual watermarking technique with multiple biometric watermarks”, Sadhana, Springer, vol. 39, issue. 1, pp. 3-26, 2014
- [29] Xiao-Long Liu, and Chia-Chen Lin, “Blind dual watermarking for color image authentication and copyright protection”, IEEE transactions on circuits and systems for video technology, 2016.
- [30] Rohit M. Thanki, Ved Vyas Dwivedi, Komal R. Borisagar, “ A watermarking technique using Discrete Curvelet Transform for Security of Biometric Features”, International Journal of Information Processing, Volume 10, issue 1, pp. 103-114, 2016.

- [31] Ohud Nafea, Sanaa Ghouzali, Wadood Abdul, and Emad-Ul-Haq qazi, “Hybrid Multi- Biometric Template Protection using Watermarking”, The Computer Journal, 2015

Comparison of EIGRP, OSPF, and RIP Routing Protocols using OPNET Simulator

Aboajela Dogman

Dept. of Electrical and Computer Engineering - Libyan Academy for Postgraduate Studies, Libya

email: Aboajela.almasri@academy.edu.ly

المخلص:

تعتبر بروتوكولات التوجيه من أهم الركائز التي تعتمد عليها الشبكات في عملية الاتصال والتحديث وتبادل المعلومات فيما بينها. تتمثل الوظيفة الأساسية لبروتوكولات التوجيه في اختيار المسار الأمثل للحزم للانتقال إلى وجهتها النهائية. جميع بروتوكولات التوجيه المستخدمة حاليًا في الشبكات الحديثة هي بروتوكولات التوجيه الديناميكي، والتي تنقسم بدورها إلى بروتوكولات البوابة الداخلية IGPs وبروتوكولات البوابة الخارجية EGP.

تستخدم IGPs خوارزمية متجه المسافة أو خوارزمية حالة الارتباط، بينما تستخدم EGP خوارزمية متجه المسار لاختيار المسار الأمثل. في هذه الورقة البحثية، تمت مقارنة أداء IGPs، وهي RIP وEIGRP وOSPF، باستخدام أداة محاكاة OPNET أظهرت النتائج أن بروتوكول EIGRP يستغرق أقل وقت للتقارب بين الشبكات، بينما يستغرق بروتوكول OSPF وقتًا أطول للتقارب. ومع ذلك، يستغرق بروتوكول RIP وقتًا أطول للعمل في التقارب.

Abstract

Routing protocols are considered to be one of the most important pillars on which networks depend in the process of communicating, updating, and exchanging information between them. The primary function of routing protocols is to choose the optimum route for packets to travel to their final destination. All routing protocols currently used in modern networks are Dynamic Routing Protocols, which in turn are divided into Interior Gateway Protocols (IGPs) and Exterior Gateway protocols

(EGPs). IGP's use the Distance vector algorithm or Link state algorithm, while EGP's use the Path vector algorithm to choose the optimal route. In this research paper, the performance of IGP's, namely RIP, EIGRP, and OSPF, was compared using the OPNET simulation tool. The results show that EIGRP protocol took the least time to converge between networks, while OSPF takes a longer time to converge. However, RIP protocol takes the longest time to work in convergence.

Keywords: RIP, EIGRP, OSPF, OPNET

1. Introduction

The primary function of a router is to forward packets from one network to another. The routing process takes place by choosing a specific path through which packets pass.

This process is performed by routing protocols, where routing protocols use specific algorithms to choose the route where packets can pass through.

There are several criteria can be used to classify routing protocols. Routing protocols can be classified into: Interior and Exterior routing protocols, Dynamic and Static routing protocols, and routing protocols that use Distance vector algorithm and others that use the Link state algorithm. Figure (1) shows the classification of routing protocols.

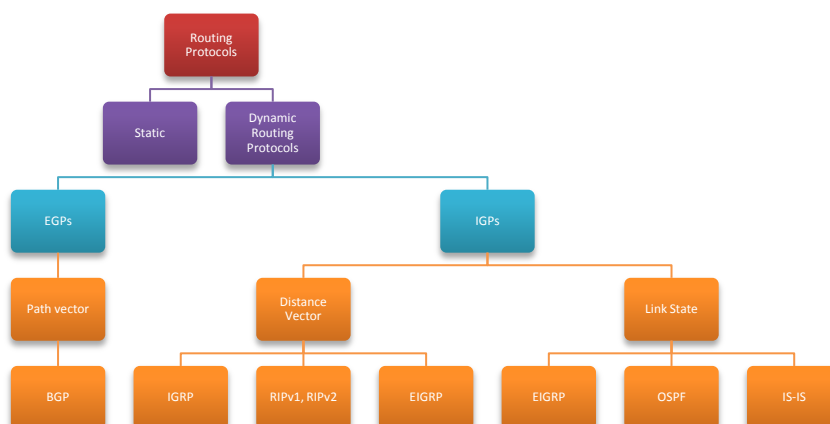


Figure (1): Classification of Routing Protocols [1]

The following subsections explain the classification of routing protocols:

1.1 Interior and Exterior Routing Protocols

This classification depends mainly on the Autonomous System (AS), AS can be defined as a group of routers, which use a specific protocol to exchange routing information inside and outside the AS. Routing protocols are divided under this classification into:

Interior Gateway Routing protocols

The IGP work within the autonomous control system (AS), as shown in Figure (2).

The most IGP are:

- ❖ Routing Information Protocol (RIP)
- ❖ Enhanced Interior Gateway Routing Protocols (EIGRP)

- ❖ Open Shortest Path First (OSPF)

Exterior Gateway Routing Protocols

The EGPs work to exchange routing information between different Autonomous Systems as shown in Figure (2). The main function of EGPs is to connect different ASs. One of the most famous EGPs is the Border Gateway Protocol (BGP).

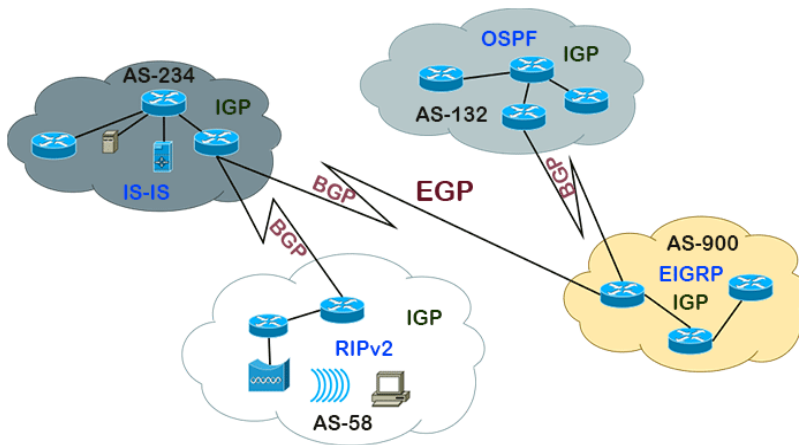


Figure (2): Interior & Exterior Routing Protocols [2]

1.2 Dynamic and Static Routing Protocols

The routing protocols in this criteria are divided into dynamic routing and static route. The network engineer sets the static route, and the router directs packets through this path without taking into account any other criteria. It is not recommended to use static routes in routing operations because they require direct monitoring by the network engineer.

Dynamic Routing Protocols choose the optimum path based on certain algorithms, either choosing the shortest path or the best path. Dynamic protocols also update routing information to determine the path through which packets will pass. The updating process takes place periodically, in order to add new networks, or find the failure of existing networks.

1.3 Routing Protocols Algorithms

Routing protocols are classified into protocols that use the Distance Vector algorithm, protocols that use the Link State algorithm, and protocols that use the Path Vector algorithm.

Protocols that use the distance vector algorithm calculate the best path based on the shortest distance through which packets can pass. The algorithm calculates the number of routers between the sending and receiving nodes, and based on the smallest number, the packet routing path is chosen. The most well-known protocols that use the Distance vector algorithm are RIPv1, RIPv2, and IGRP.

Protocols that use the Link State algorithm calculate the best path based on a set of criteria, including bandwidth and delay coefficient, depending on the type of protocol. The most famous protocols that use the Link State algorithm are OSPF and IS-IS.

Protocols that use the path vector algorithm calculate the path based on the vector distance and available path information. The Path vector algorithm is used in (EGPs). The most famous EGP is BGP.

In this research paper, the focus will be on the comparison between the performance of RIP, OSPF, and EIGRP in terms of their capability for network convergence.

2. Routing Protocols

This section explains in some detail the IGPs: RIP, EIGRP, and OSPF, as the aim of this paper is to compare the performance of these protocols.

2.1 Routing Information Protocol

This protocol is considered to be one of the interior dynamic routing protocols that uses the Bellman-Ford routing algorithm, which is one of the algorithms that relies on calculating the shortest path to direct packets.

This protocol employs a counter to avoid the problem of counting to infinity by defining a maximum number of permissible distances, which is 15 routers, which limits the size of the network supported by this protocol, and is suitable for small networks.

RIP works at the network layer, and it uses one table, which is the Routing Table, in which network addresses and routes are recorded, and it calculates the best path through the least number of routers.

RIP sends routing table updates every 30 seconds to routers that work with it. RIP has two versions, RIPv1 and RIPv2. [1]

2.2 Open Shortest Path First

OSPF is classified as a link state routing protocol and was developed by the Internet Engineering Task Force (IETF) to be an alternative to the RIP protocol. [3]

The OSPF protocol creates three tables:

- Neighbor table: it includes all information about neighboring routers.
- Topology table: it contains a complete map of the network, including available OSPF routes and alternative routes to the best route if it is not available.

- Routing Table: it includes the best path under the current situations, which will be used to direct traffic between neighboring routers.

2.3 Enhanced Interior Gateway Routing Protocol

The EIGRP was developed by Cisco and it is an improvement to the IGRP protocol. EIGRP is a hybrid protocol that has characteristics of protocols that use the Distance vector algorithm and protocols that use the Link state algorithm. EIGRP uses the Diffusing Update Algorithm (DUAL), which uses metrics such as bandwidth and delay to calculate the optimal path.

EIGRP has fast convergence and updates using specific information about available routes. The number of hops in the EIGRP protocol reaches 255 hops. The EIGRP protocol has three tables containing information about available routes. These tables are:

- Neighbor Table: This table includes information about the routers that are directly connected to the router that has the EIGRP protocol enabled.
- Topology Table: This table contains all information about the networks associated with neighboring routers
- Routing Table: It contains all the routes available for networks associated with routers that have the EIGRP protocol enabled.

Figure (3) shows the process of building relationships with neighbors and how to build an EIGRP protocol table

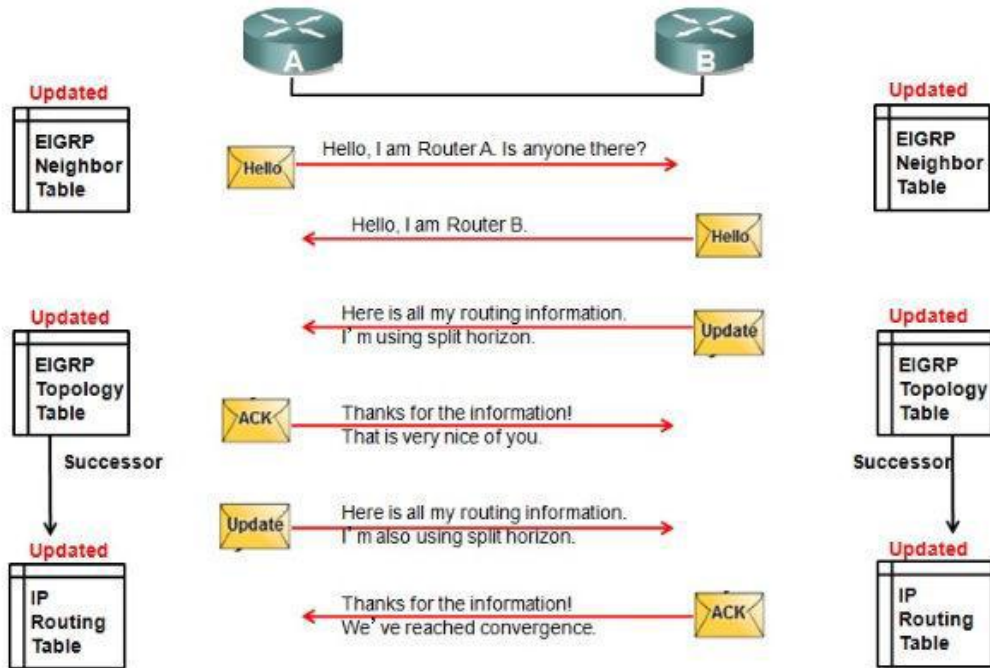


Figure (3): The process of building EIGRP tables [3]

3. Related works

There are many previous studies that have been conducted regarding comparing the performance of interior routing protocols RIP, OSPF, and EIGRP. For example: Researchers in [3] compared routing protocols RIP, OSPF, and EIGRP in terms of quality of service on physical (real) networks.

On the other hand, in 2014, researcher Gehlot and others in [4] evaluated the performance of the RIP, OSPF, and EIGRP protocol using several criteria, including the delay coefficient and the rate of sending and receiving packets.

In 2012, S. Farhangi and others in [5] analyzed and compared networks using routing protocols OSPF, IS-IS, and EIGRP. The comparison was analyzed using voice and video packets, and the results showed that the convergence coefficient for IS-IS, OSPF is lower than the convergence coefficient for EIGRP.

In this paper, the comparison of routing protocols RIP, OSPF, and EIGRP will be carried out using OPNET.

4. Research methodology

In this research paper, we compared the performance of routing protocols RIP, OSPF, and EIGRP using the network simulation tool OPNET. A deductive research approach was employed using experiments to compare and evaluate the performance of the aforementioned routing protocols. The next sections provide an explanation of the OPNET simulation tool and network topology.

4.1 OPNET Simulation Tool

OPNET stands for Optimized Network Engineering Tool, which is a computer network simulation program provided by OPNET Inc. It supports communications in wired and wireless networks. [6]

OPNET has licensed version, which is OPNET Modeler, and a free version, OPNET IT Guru, which is used for academic purposes and scientific research purposes, with limited capabilities. OPNET can be downloaded directly from the company's website for free. OPNET has many features which can be summarized as follows:

1. Provides a graphical user interface GUI.
2. Easy to use compared to other simulation tool such as NS-2.
3. Compatible with wireless networks.

4. It does not require programming skills when using it.
5. There is a free version of OPNET.
6. High degree of accuracy of simulation results.
7. Linking with Excel to analyze the results and draw them according to the user's needs.

4.2 Experimental Procedure

In this paper, the network was simulated using the OPNET program, which contains 5 subnetworks connected to each other with 3 scenarios as follows: in the first scenario, RIP protocol was activated, in the second scenario, OSPF protocol was activated, and in the third scenario, EIGRP was activated. The simulation period took about 900 seconds. The application sent during the simulation period was video. Figure (4) shows the simulated network.

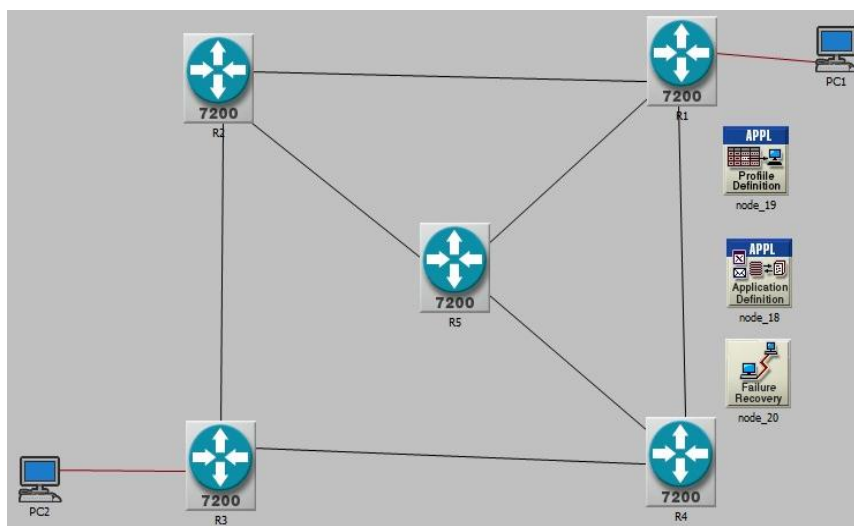


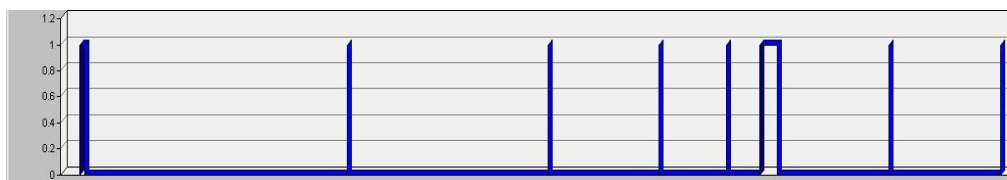
Figure (4): Network Topology

During the simulation period, network malfunctions occurred from time to another through the Failure recovery tool. The following table shows the time periods during which network malfunctions occurred and the periods during which the network returned to operating normally.

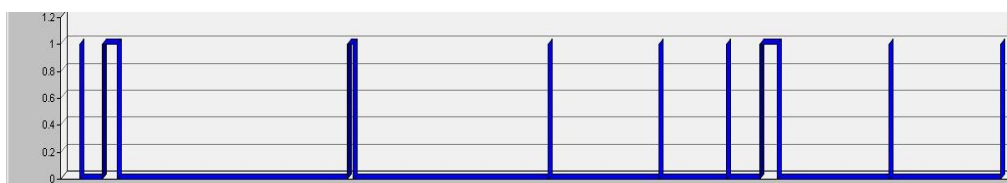
Status	Fail	Recover	Fail	Recover	Fail	Recover	Fail	Recover	Fail	Recover
Time (seconds)	240	420	520	580	610	620	625	626	726	826

5. Results and Discussion

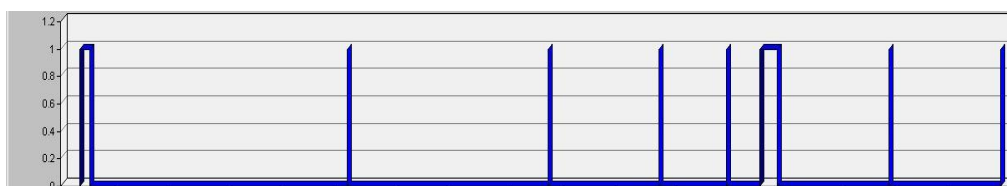
In this paper, several criteria were used to compare the performance of routing protocols RIP, OSPF, and EIGRP. However, one of the most important parameter that considered in this paper is Network convergence. Network convergence tests how fast the routing protocol gather, update, and broadcast the routing information. Network convergence was measured according to network activity which fluctuated between failure & recovery as shown in Figure (5)



Network Convergence Activity - EIGRP



Network Convergence Activity - OSPF



Network Convergence Activity - RIP

Figure (5): network activity: (a) EIGRP, (b) OSPF, (c) RIP

Figure (6) shows the comparison between RIP, EIGRP, and OSPF in terms of network convergence. From the figure, it is noticeable that EIGRP took the least time to converge between networks, while OSPF took the longest to converge, whereas RIP protocol took the longest to converge.

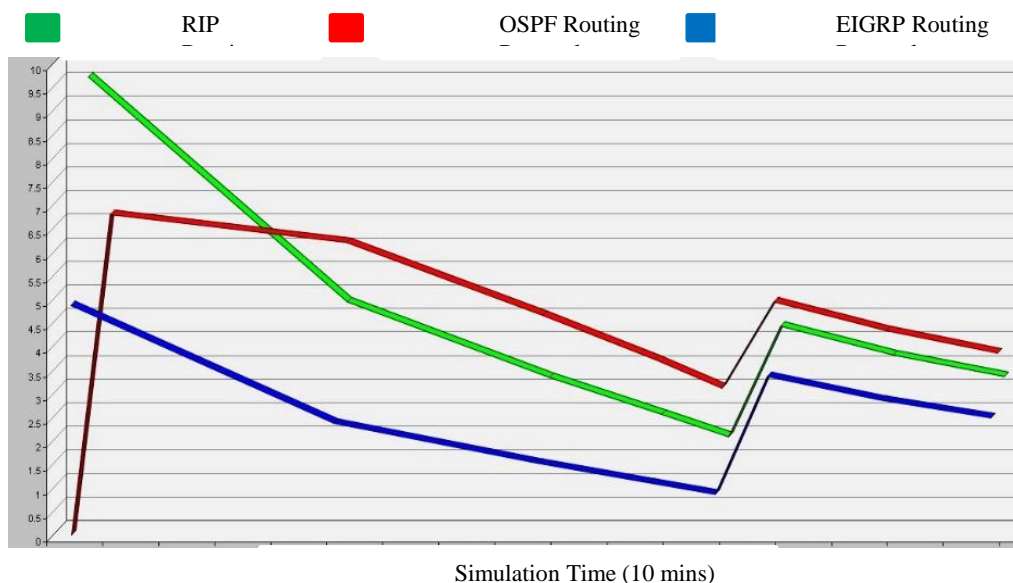
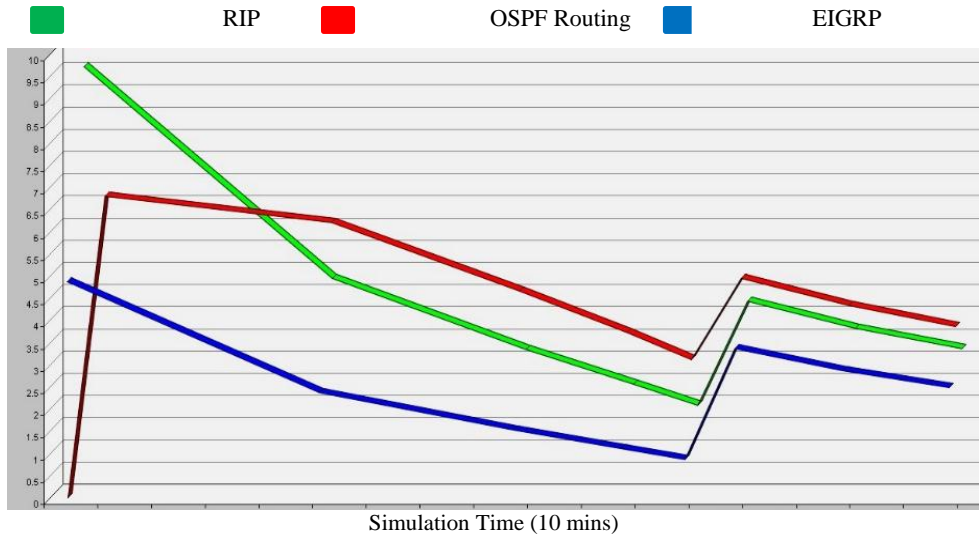


Figure (6): network convergence scenarios for RIP, OSPF, and EIGRP

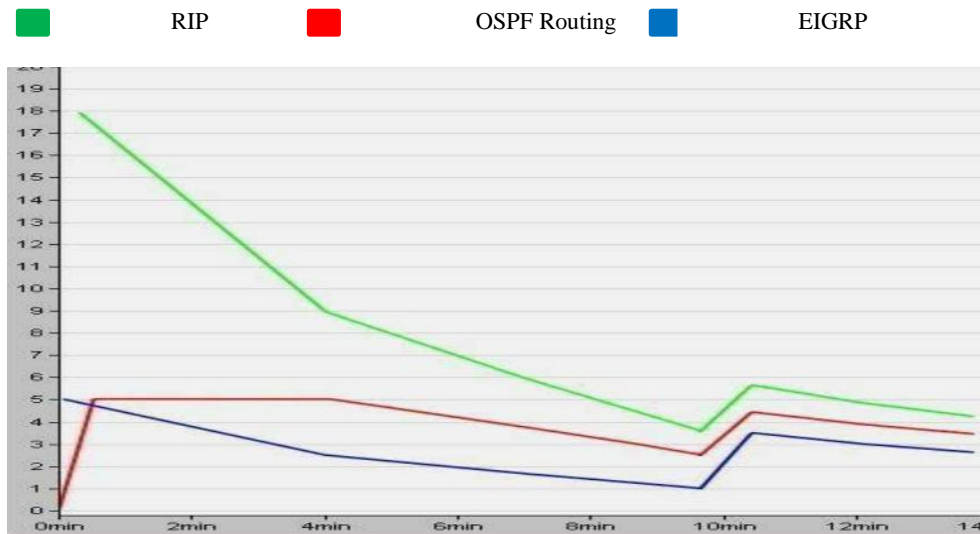
These results are consistent with the results obtained by researchers in [7] who used the convergence coefficient and data transmission rate to compare the performance of routing protocols.

The results obtained were also compared with the results obtained by [1] who used the convergence coefficient, channel utilization coefficient, and delay coefficient to compare EIGRP, RIP, and OSPF. From the comparison, it is clear that the obtained results are consistent, and relatively convergent as shown in Figure (7).

The other comparison was made with results obtained by researchers in [8] The comparison clarifies that both results are similar and comparable as shown in Figure (8).

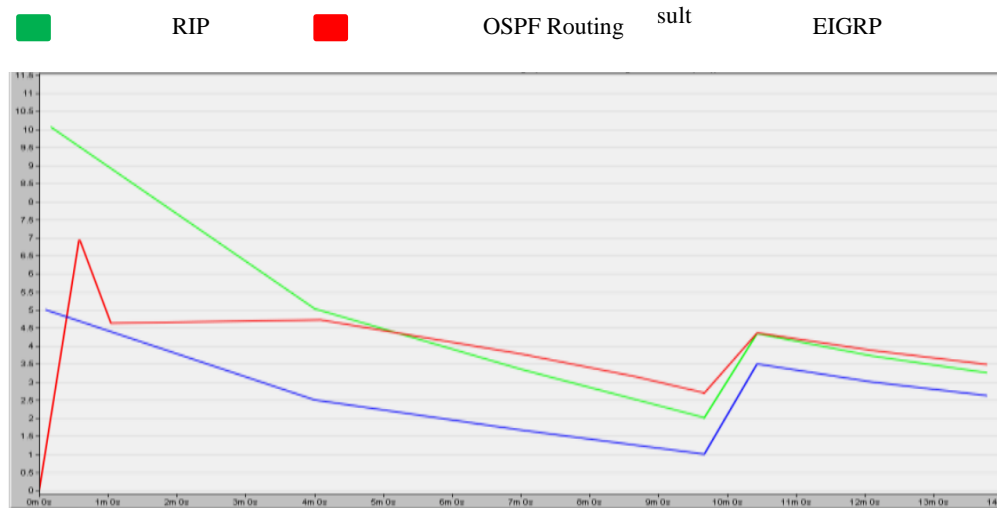
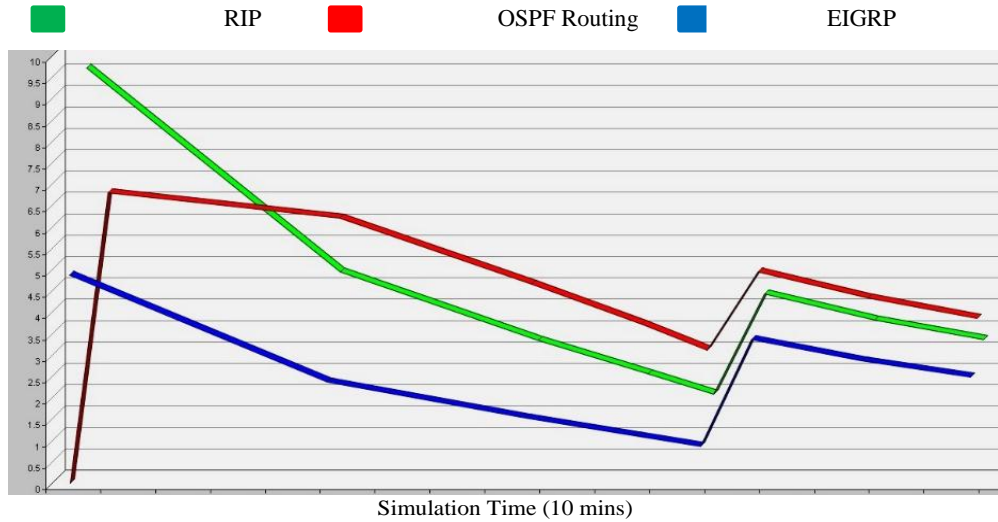


(a) Network Convergence results obtained



(b) Network Convergence results

Figure (7): comparison of (a) obtained results with (b) results obtained by [1]



(b) Network Convergence results

Figure (8): comparison of results with results obtained by [8]

As shown in Figures (7) and (8), it is clear that the researchers used network convergence to compare routing protocols. The results in Figures (7) and (8) prove that EIGRP protocol does not take longer to converge between networks, while OSPF takes a longer time to converge. However, RIP protocol takes the longest time to work in convergence.

6. Conclusion

In this paper, the performance of the most famous internal protocols, namely RIP, EIGRP, and OSPF, was compared by relying on the results of previous studies, which in turn used the OPNET simulation program for comparison. The results showed that the EIGRP protocol does not take longer to converge between networks, while OSPF takes a longer time to converge. However, RIP protocol takes the longest time to work in convergence.

7. References

- [1] Comparative assessment Analysis of RIP, OSPF, and EIGRP Routing Protocols using OPNET. International Journal of Management, IT and Engineering, 5(7), pp.1-17.
- [2] IGP, EGP, and Autonomous System available at: <https://www.computernetworkingnotes.com/ccna-study-guide/igp-egp-and-autonomous-system-explained.html>
- [3] Shafiul , H., Khan, M. N., Nazrul Islam, M., & Ashique, M. A. (2013). Performance Evaluation of Dynamic Routing Protocols on Video Streaming Applications. Current Trends in Technology and Science. Karlskrona, Sweden: Current Trends in Technology and Science.
- [4] Gehlot , K., & Barwar, N. (2014). Performance Evaluation of EIGRP and OSPF Routing Protocols in Real Time Applications. International Journal of Emerging Trends & Technology in Computer Science (IJETTCS).

- [5] S. Farhangi, A. Rostami , & S. Golmohammadi. (2012). Performance Comparison of Mixed Protocols Based on EIGRP, IS-IS and OSPF for Real-time Applications. Middle-East Journal of Scientific Research.
- [6] OPNET, last accessed on 22/02/2024 at: <https://support.riverbed.com/content/support/software/opnet-model/modeler.html>.
- [7] [7] Hossain, M.A., Ali, M.M., Akter, M.S. and Sajib, M.S.A., 2020. Performance comparison of EIGRP, OSPF and RIP Routing protocols using cisco packet tracer and OPNET simulator. Global Journal of Computer Science and Technology.
- [8] Xu, D. and Trajkovic, L., 2011. Performance analysis of RIP, EIGRP, and OSPF using OPNET.

Video game development on Roblox platform using Lua programming language

Sumaia A. Eltomi ¹, Rasheed S. Mottaleb ²

^{1,2}Dept. of Electronic, College of Industrial Tech, Misurata, Libya

Somaia_ali@cit.edu.ly ¹

المخلص

هذه الورقة تهدف إلى شرح عملية تطوير ألعاب الفيديو للمبتدئين، بما في ذلك تعلم البرمجة والتصميم، وإتمام عملية التطوير بشكل صحيح. تناقش الورقة الافتراضات الخاطئة في عملية التطوير وكيفية تجنبها، بالإضافة إلى المكونات الأساسية لأي لعبة. كما تغطي اختيار المحرك ولغة البرمجة المناسبين استنادًا إلى فئة اللعبة المستهدفة وعملية نشر اللعبة. تتناول الورقة أيضًا لغة لوا وعلاقتها بتطوير الألعاب، مع التركيز على استخدامها في منصة روبلوكس. الجانب العملي للورقة هو عملية نشر اللعبة على هذه المنصة. تستنتج الورقة أن الأفراد الذين يمتلكون خبرة في التصميم والبرمجة يمكنهم تطوير ألعاب فيديو عالية الجودة.

Abstract

This paper aims to explain the process of developing video games for beginners, including learning programming and design, and completing development correctly. It discusses misconceptions in the development process and how to avoid them, as well as the basic components of a game. It also covers selecting the appropriate engine and programming language based on the target game category and the game publishing process. The paper reviews the Lua language and its relationship to game development, with a focus on its use in the Roblox platform. The practical aspect of the paper is the process of publishing a game on the platform. The paper concludes that anyone can develop video games, but higher quality and greater flexibility in the game are achieved as developers gain experience in design and programming.

Keywords: Video game, video game development, Lua language, Roblox studio.

I. INTRODUCTION

Video games are interactive experiences enjoyed by players in virtual worlds filled with exciting stories and challenges. They include multiple genres such as action, adventure, sports, and shooting games. Advanced graphics, sound, and artificial intelligence technologies are used to create a realistic experience that captivates players and transports them into the game world. Players can interact with characters and environments and make decisions that affect the course of the game. Some games offer educational experiences that contribute to gaining knowledge and developing skills. Furthermore, companies use gaming as a marketing tool. Video game development is the process of creating and designing video games through software development. Video game development is undertaken by either individuals or large companies. Funding for well-known games is usually provided by publishers, and development times can vary. Indie games, on the other hand, can be produced by individuals or small developers and may require less time to develop. The indie game industry has experienced significant growth in recent years, thanks to the rise of new network distribution systems and the mobile game market. [1].

Video game development involves several stages. It begins with conceptualization and design, where developers brainstorm ideas, create game mechanics, and design characters and environments. This phase sets the foundation for the entire development process. Once the design is finalized, production begins. This involves creating game assets, such as 3D models, textures, animations, and audio elements [2]. Programmers write the code that brings the game to life, implementing mechanics, interactions, and artificial intelligence systems. This requires expertise in programming languages and game engines. [3].

Testing and quality assurance are crucial in ensuring the game is free from bugs and glitches. Testers play through the game meticulously, identifying any issues and providing feedback for improvement [4]. The visual and audio aspects of the game are vital for creating an immersive experience. Graphic designers create stunning visuals, while sound designers craft the audio elements. These elements contribute to the emotional impact of the game. [5].

After completing the development phase, the game undergoes a final round of testing and polishing. Then, marketing strategies are devised to promote the game. Video game distribution has evolved significantly in recent years. While traditional methods include physical copies sold in retail stores, digital distribution has become popular. This has opened up opportunities for independent developers to showcase their creations and reach a wider audience.

The paper is structured as follows: Section II provides an overview of related works in game development. Section III discusses the pre-development process, Section IV addresses game programming languages, Section V introduces Roblox Studio, Section VI summarizes video game development methodologies, and the final section summarizes the research results

II. RELATED WORK

Numerous academic studies have been conducted on game development in recent years. However, for our purposes, we will focus on the most relevant studies, which are discussed in this section.

This paper explores the use of video game engines, specifically the Roblox Studio engine, to create a virtual simulation of sculptural heritage in a classroom setting. A pilot experiment was conducted with 53 high school students who designed a virtual environment featuring 3D models of the sculptural heritage of a specific city. Students reported an increased awareness of the city's sculptural heritage and felt confident in their ability to create interactive worlds using Roblox [6].

The research paper explores moderating user-generated virtual worlds (UGVWs) on platforms like Roblox. It addresses issues with harmful user-generated content and the complexity of moderating game design. The study examines the impact of harmful design on Roblox users, identifying potential risks such as inappropriate content and problematic incentive mechanisms. It also discusses the opportunities and challenges in mitigating these issues [7].

In their study [8], the authors explore the potential benefits and opportunities of incorporating Roblox into university courses as an educational tool. They examine its impact on higher education and address the challenges faced by students and teachers in this context. The literature review highlights the limited exploration of Roblox's potential in higher education thus far. The aim of this research is to investigate students' views on the integration of Roblox as an educational tool using the TAM model.

A previous study [9] explored the use of digital games in a learning context, with a particular focus on game design strategy. The study highlighted the potential of Roblox technology to enhance the learning process. However, the article notes that the current evidence is mainly descriptive, and there is a lack of comparative studies and evidence-based frameworks. The article concludes with an analysis and review of current evidence, without presenting direct findings from original research. Based on the analysis, the article draws some observations and suggests future directions.

The paper analyses the requirements of metaverse platforms and evaluates existing platforms to determine their ability to meet those requirements. It discusses the growing interest in virtual worlds, also known as metaverse, in an objective manner. The text highlights the limitations of these platforms and identifies the need for further research and development in areas such as pervasive thinking, security and privacy, and integration of emerging technologies like blockchain and artificial intelligence. To build a robust and secure metaverse in the future, it is recommended to pay more attention to these aspects. [10].

This paper examines the use of ChatGPT in creating educational and interactive environments within the Roblox metaverse. The study shows how ChatGPT streamlines the development process by optimizing scripts, creating well-structured dictionaries, and simplifying the implementation of effects and interactions. College-level student testing demonstrated that integrating ChatGPT improved student engagement and understanding, indicating its potential for developing metaverse-based educational content [11].

In a study by researchers [12], the use of the game Roblox as an educational tool in Indonesia was discussed as a means of improving second-grade students' digital multimedia literacy abilities. The results showed the importance of using Roblox as a positive educational method to improve students' digital multimedia literacy abilities. The research concludes that lesson design for middle school English teaching should incorporate the use of games as a teaching tool.

III. PRE-DEVELOPMENT EXPLORATION

New game developers often make the mistake of relying solely on online videos and attempting to create games sequentially without a sufficient background in game development basics. This approach often results in the development of undistinguished games that fail to meet player needs and expectations. New developers may become distracted and frustrated when they do not achieve satisfactory results quickly. To avoid this problem, they should research common mistakes in game development and how to avoid them, as well as follow the essential steps to learn the basics. [13].

A. Hidden Challenges

Aspiring game developers encounter challenges beyond technical and creative skills. It is crucial to address common mistakes when designing their first game.

- Cloning a game without any innovation significantly diminishes its value.
- Randomly incorporating artistic elements affects game's attractiveness Figure1.
- Game size and complexity: Novice developers may struggle to create large and complex games, which can negatively impact game quality.
- Imbalanced speed negatively impacts the player's experience and ability to challenge.
- Matching the difficulty of a game with the target group of players is crucial for a positive game experience.
- Early criticism before completion can negatively impact the game's quality and cause frustration.
- It is important to focus on learning the basics before adding details and stages.

- Bias towards the game can lead to false sentiment and affect its quality and acceptance.
- To meet the needs of players, it is important to focus on a specific category rather than trying to satisfy everyone.
- Instant success is not guaranteed, so it is important to come up with a new idea that aligns with the interests of players, as demonstrated in the games in Figure2.



Figure 1: Random merging of graphics


















Figure 2: Famous games

B. The resources

Game resources are essential for creating a unique and engaging user experience. By customising resources independently, developers can create more distinctive games.

- Game development ideas can come from various sources, and the success of a game depends on its design concept. To generate ideas for game development, one can analyse existing games, draw inspiration from different media such as books and movies, or explore a specific concept through game design. For instance, an educational game about the environment can be created. Players' interests can be met while providing a fun experience. Experienced developers can be consulted for their knowledge and guidance in this field. [14].
- Developers often have limited resources when it comes to models and graphics, especially in the early stages. However, there are many websites that offer free game assets, as shown in Table1. These resources can provide a variety of visual elements that can be used in game design.

Table 1: Website and store free artwork

 CraftPix	 Kenney	 Poly Haven	 DOTOWN	 Super Game Assets
 Game Art 2D	 Quaternius	 Textures	 itch.io	 Unreal Engine Marketplace
 Gamefresco	 OpenGameArt	 GameDev Market	 Unity Assets Store	 Reddit Free Game Asset Forum

- Beginner programmers can find reclaimed code online through code-sharing websites and online programming communities. These resources offer ready-made code for specific functions and programming instructions that can be modified to meet specific needs. Table 2 displays ready-made coding sites.
- Code sharing enables programmers to share their code with others for debugging, education, or collaboration. Numerous code-sharing websites exist on the web, where programmers can interact and share experiences. Table 3 lists some of the most important of these websites.
- Sound sources: Independent developers have access to a variety of free sound effects and music for their games. They can find these resources on comprehensive audio databases or genre-specific blogs, such as those listed in Table 4. Utilizing these resources can help developers add creative and suitable sound and music to their games.

Table 2: Code snippets





 GenerateWP	 CodePen
 StackOverflow	 chatGPT

Table 3: Code Review





 Github Gist	 JS Bin
 JSFiddle	 Codeshare

Table 4: Free Sound Effects

 Freesound	 Soundjay
 Game Burp	 99 Sounds

C. The game engine

Game development software includes a store app, a publishing platform, and tools essential for development. Choosing the right engine is crucial for novice developers, considering game type, device requirements, budget, and other factors. The selected engine significantly impacts team capabilities and project progression, varying with game diversity. These six factors are crucial for engine selection. [15].

- The choice of game engine should be based on team's skills and the ready time.
- Team size: Some engines can be used alone, while others require collaboration.
- The cost of game engines varies by type and features. Free engines are accessible, but advanced features may necessitate a subscription or purchase, while paid engines usually require a subscription fee or outright purchase.
- Programming skills: The ability to write basic and object-oriented coding, graphics, sound, AI development, visual programming and databases.
- Game Type: Select an engine that supports your desired game type and provides tools and features to facilitate the creation of various game types.
- Final Product: Game development assesses project scope and target platform compatibility. Engine choice varies; smaller games like mobile or web games can use different engines, while larger 3D games require more powerful options.

There are many popular game engines widely used in the industry. Table 5 compares the characteristics of Roblox, Unity, Unreal, and Godot and evaluates whether they are advantageous or disadvantageous.

Table 5: Characteristics of game engines

	Roblox ^[16]	Unity ^[17]	Unreal ^[18]	Godot ^[19]	
Platforms	Multi	Multi	Multi	Limited	
	Huge	Big	Big	Limited	Audience
Correction	Easy	Easy	Learn C++	Difficult	
	One	Team	Team	One	Developers
Graphics	Good	Medium	High	Good	
	Free	Almost free	Not free	Free	license
RAM usage	Acceptable	High	Very high	Acceptable	
	Lua	C#	C++	GDScript	language
Lead time	Short	Moderate	long	Moderate	
	Enable	Enable	Not enable	Enable	Live-editing
Popular games	Most	Moderately	Moderately	Less	
	More users	Independent	companies	Less used	Users
Exp. Required	Less	High	High	Moderate	
	Easy	Moderate	Moderate	Moderate	Usability
Community	Strong	Strong	Average	Weak	
	Dependent	independent	independent	independent	Independence
Profit sharing	Weak	NA	NA	NA	

This table provides an overview of the advantages and disadvantages of different engines. Ratings may vary depending on the needs and requirements of the developer and their project. It is recommended that developers try and compare different engines to choose the most appropriate one for their project.

D. Publishing

Publishers play a crucial role in the gaming industry by publishing, marketing, and investing in games. They offer a range of services, including advising and managing game development, financing, distribution, and marketing across various channels [16].

In the video game industry, publishers provide assistance in game production financing, marketing strategies, and product plan development and support. Publishers use various techniques to enhance the effectiveness of games, such as distribution and advice. They also handle tasks like obtaining licenses, writing guides, and creating visual elements. Without the help of a publishing company, these tasks can be difficult or even impossible for small publishers.

IV. GAME PROGRAMMING LANGUAGES

A game programming language or script is the system that game programmers use to shape game settings and environments. It is the mechanism that makes a video game work in a specific way. Game programming languages vary in complexity and power. Some are simple and easy to learn, designed to produce quick-to-build games, while others are more complex and allow programmers to create highly sophisticated and intricate games.

Programming languages have specific purposes and structures that make them more efficient at certain tasks. Although they may overlap and be compatible with each other, programmers developing games often use a variety of languages. [17].

The choice of programming language for game development depends on various factors, such as the game type, target platform, and complexity [18]. Table 6 displays some of the frequently used programming languages in video game development.

Table 6: Popular game programming languages

Key Programming Languages in Game Development		
	Compatible with games, small projects, web applications, and image processing.	Lua
C++	Powerful for developing high-quality video games, and efficient memory management.	
	Powerful for video games, relatively easy to learn, popular among novice programmers.	C#
java	The product is versatile and can be upgraded, making it competitive in the modern technology industry.	
	Popular in browser-based game development and web-based games.	JavaScript
Python	It is based on object-oriented programming and facilitates the creation of prototypes.	
	Exclusive to mobile operating systems, such as Android and iOS.	Objective-C

A. Lua programming language

It was inspired by SOL (Simple Object Language), and named after the Portuguese word for 'moon'. The team of professors chose the name 'Lua' for the new language, as it means 'moon'. Figure 3 displays the official logo for the Lua programming language. Lua is a dynamically typed scripting language that is composable. The code in Lua is read line by line, from top to bottom, making it easy to read and write. [19].



Figure 3: Lua Official logo

Lua is an exceptional language due to its design as an extension language that can be integrated into any platform or application. This allows developers to fully customize products. Additionally, Lua can handle any C and C++ code, making it easy to create new game systems. Lua programs are small, flexible, and portable, making them an ideal starting point for extending various types of programs. [20].

Lua is a versatile programming language that is commonly used in gaming and web development. It has been used in a variety of applications, including the mobile payment app Venmo and the popular game Angry Birds. Overall, Lua's flexibility and compatibility make it a valuable tool for developers and designers alike. Additionally, Lua is a popular choice for game developers on platforms such as Roblox, where it is used to write code for creating new games. Designers can also create plug-ins for image editing software Adobe Lightroom using Lua. [21].

B. Concepts and Fundamentals

To become proficient in Lua, the programmer must first explore its syntax and become familiar with its basic concepts and terminology. Starting with simple commands, they can gradually progress to more complex instructions, gaining greater control over the language and using it more professionally.

- **Variables in Lua:** A variable is a value that can be altered throughout the program. The value of the variable can be stored and referenced in later sections of the program [22]. Lua requires variables to be declared before use,

and variable names are case sensitive. For instance, 'Rody', 'rody', and 'RODY' are distinct variables in Lua. Refer to Figure 4 for additional information on Lua variables.

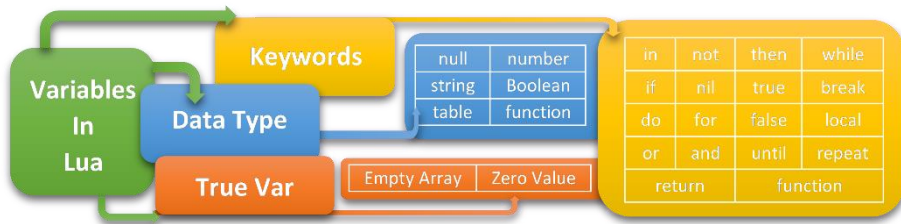


Figure 4: Variables in Lua

- **Functions in Lua:** A function is a group of statements that carry out a particular task. Functions help to break down code into clear and understandable units, with each function performing a specific task within the program. [23]. The Lua programming language defines functions in the general form shown in Figure 5.



Figure 5: Official logo of the Lua language

- **Lua in game engines:** Lua programming language is used by many game engines. This does not imply that the engine was created in Lua, but rather that it supports Lua as a programming language [24]. Table 7 and Table 8 include 2D and 3D game engines respectively.

Table 7: Exploring 2D Games with Lua-Powered Engines

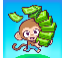







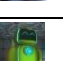
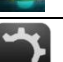

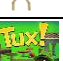
Icon	Ex; game	2D Lua Engines:	Engines
	Monkey Mart	This engine is built using a component-based system for optimal performance.	Defold
	Rider	This cross-platform framework is perfect for developing and publishing games across mobile, TV, and PC.	Corona
	Move or Die	This is an open-source and free Lua framework for 2D games that is compatible with various operating systems.	LÖVE
	Sweet Combo Match	The engine is a free and open-source technology that enables the creation of amazing games across multiple platforms.	Gideros
	cat vs Roomba	This software library is designed for programming video games with a simple interface and no additional tools beyond programming.	Raylib
	Aeroplane Adventure	This tool is designed to create text-based games that combine interactive fiction, narrative, and visual elements.	Instead

Table 8: Exploring 3D Games with Lua-Powered Engines

Icon	Ex; game	3D Lua Engines:	Engines
	Zero-K	Versatile and fully customizable, including the GUI.	Spring RTS
	Racing Fever	This software provides powerful features for creating, playing, and sharing games on a PC without requiring any prior programming knowledge.	GameGuru
	Kumoon	This software offers all the features of contemporary 3D games, such as resource management, scenery, and user interface.	Shiva
	Leadwerks	Provides a smooth learning curve for beginners to become professional game developers with ease.	Leadwerks
	RSM game	The practical part of this paper will be reviewed later.	Roblox Studio
	Tux!	This is a lightweight and free game engine that supports both 2D and 3D graphics.	Urho3D

V. ROBLOX PLATFORM

Roblox is an online gaming and game creation platform with over 40 million user-generated experiences. Users can create and share their own experiences.

Roblox is a social gaming network within the metaverse, allowing users to communicate and interact with others. Developers using Roblox Studio must use the Lua programming language to create 3D games. The software provides templates and components to facilitate game creation. [25].

A. User interface

Roblox Studio has a beginner-friendly interface that simplifies game development and provides customizable templates. The platform enables easy importation of shapes, models, and sounds, as demonstrated in Figure 6.

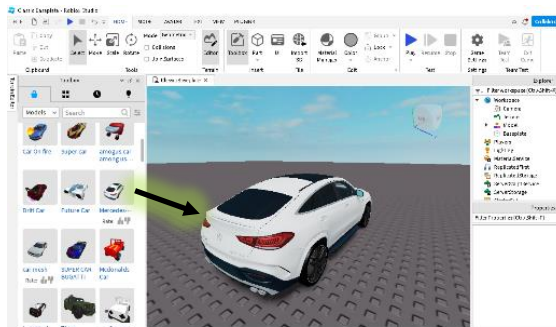


Figure 6: Importing in Roblox Studio

B. Design pattern in Roblox

The game model floor demonstrates Roblox's design approach, which was created by implementing a sequence of operations on shapes. Figure 7 shows the overlapping cylinders prior to the execution of these operations. The island model in Figure 8 was produced after further processing of the components.

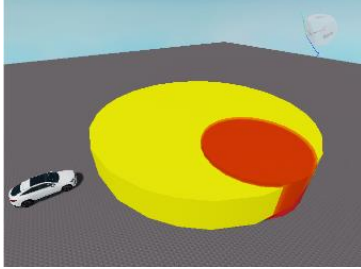


Figure 7: Two overlapping cylinders

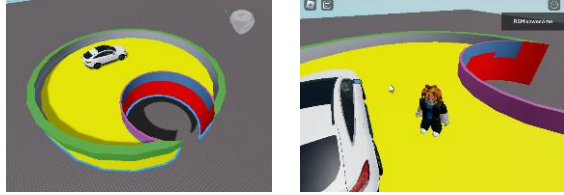


Figure 8: Island prototype

C. Integration with Lua

Game design requires time and effort. However, the game remains incomplete until programming statements define its behavior. Roblox Studio uses Lua.

To link an object, the user clicks "+" and selects "Script," opening a new programming window Figure 9.

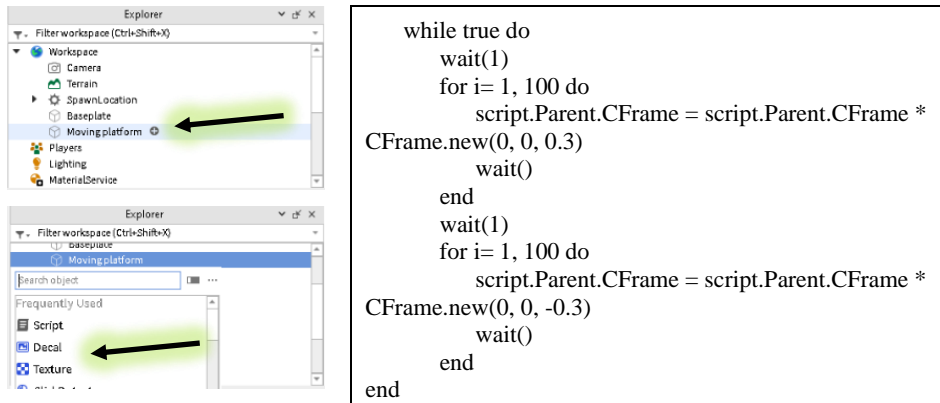


Figure 9: Adding a Lua file

D. Game testing

Game testing is a crucial development stage. It allows evaluating the design and programming, identifying issues, and demonstrating the product.

Roblox developers have two testing methods available, shown in Figure 10.



Figure 10: Game testing in Roblox

VI. GAME DEVELOPMENT METHODOLOGY

This section outlines the proposed method for the developed game, featuring two worlds: one for entertainment and the other for adventure and combat. The method includes conceptualizing the game idea, importing necessary models using Roblox, programming game behavior in Lua, designing a unique icon and cover for server login, and concluding with testing and documentation. Figure11 displays the development method.

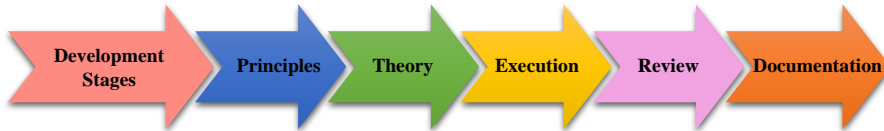


Figure 11: Game Development Stages

A. Game Principles

It involves clarifying the main ideas and features of the game, determining the sequence of events and basic elements. Game planning is a crucial process in game development. The following factors are considered in game planning:

- Define the game's objective and desired player experience.
- Create a map of the game world and label distinct areas and levels.
- Arrange challenges and stages in a consistent sequence.
- Identify characters and design their unique abilities and skills.
- Analyse preliminary layouts to identify potential issues.

The initial layout of the proposed game is shown in Figure 12.



Figure 12: The proposed game layout

B. Game Theory

The design phase begins after planning. Import required items through Roblox, selecting desired items and checking for programming files as needed. Place forms in locations outlined in the planning document.

The spawn point, where players first appear and can return to in case of loss, is set by clicking the publishing board and placing it in the game world, as shown in Figure 13. This supports development, particularly testing, and the spawn location can be changed.

Figure 14 shows creating castle rooms using merging and removing, adding effects to enhance the fantasy appearance. One room was converted to a cloud room, with the clouds serving to provide lighting and a scattered object effect, as in Figure 15.

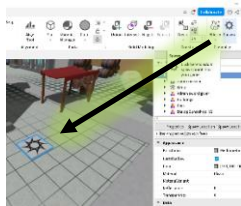


Figure 13: Create a spawn

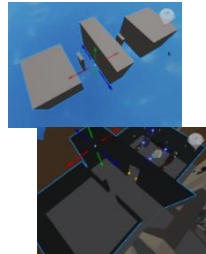


Figure 14: Create rooms and corridors

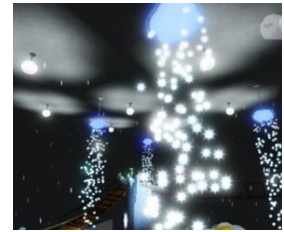


Figure 15: Effects in clouds room

The room serves as the entrance to the second world. Navigation boards are used for teleportation to the second world. There is a painting in the room and another in the second world. However, a problem has arisen as the character keeps moving back and forth between the two worlds. The touch and sensor feature were removed from the second panel. Both panels were made 100% transparent. The first panel was

placed on the door in the clouds room to create the illusion that the door is responsible for the transfer. Figure 16 displays the panels before and after transparency.

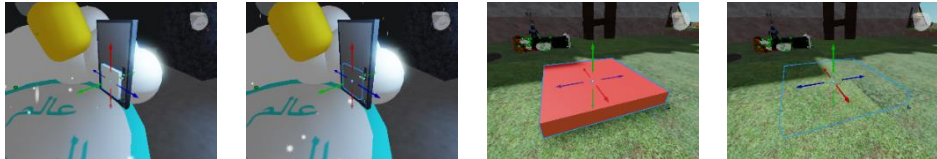


Figure 16: Transition between worlds

- Characters

The second world comprises two islands in the sky, as shown in Figure 17. One can move between them using a group of small clouds:

Weaponry Isle: This is a location for practicing exploration, shooting, and aiming. It is recommended to limit the number of weapons in the game and avoid making them easily accessible to create a challenge. To reach the next monster island, players must jump on moving clouds that travel from point A to point B. Figure 18 displays the programming file for one of these moving clouds, as shown in Figure 19.

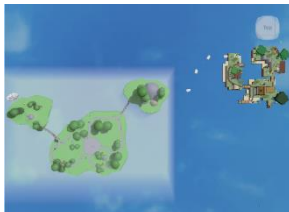


Figure 17: Second world in-game

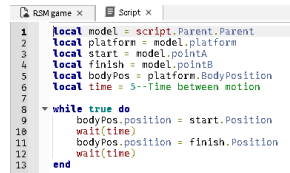


Figure 18: Animated clouds programming file



Figure 19: Moving clouds between two islands

Monsters Isle: It contains three types of monsters:

- Cloud Fairy: was imported and modified, and a machine gun was integrated into it.
- Spider: Three copies are included, each with the ability to move and multiple attack options. Adjustments have been made to their size, sound, and life points.
- Samurai: He is the leader in this world and possesses multiple software files. Despite recent changes that have reduced its speed, it remains very fast and difficult to evade. Defeating him requires a team effort. Figures 20, 21, and 22 depict the monsters.



Figure 20: Monster: fairy

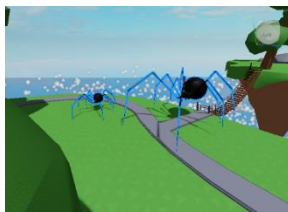


Figure 21: Monster: spiders



Figure 22: Monster: Boss

A cube has been created beneath the sky islands, as depicted in Figure 23. Its purpose is to end the player's life points and return them to spawn upon falling. The program file below should be added to the cube.



Figure 23: Transparent cube under the sky islands

```
function onTouched(hit)
    local human = hit.Parent:FindFirstChild("Humanoid")
    --Basically this just checks to see if it is a real player
    touching this brick.
    if (human ~= nil) then --If it is a real player, then
    DESTROY THEM!
        human.Health = 0 --Your Health Is Now 0.
    end
end
end
if (script.Parent ~= nil) and (script.Parent.className ==
"Part") then --Work if in a block
    connection =
    script.Parent.Touched:connect(onTouched)
end
```

- Challenges and Excitement

Figure 24 shows the most important challenges that have been undertaken.

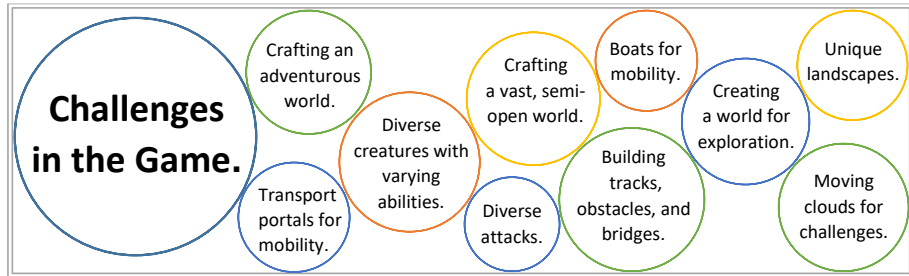


Figure 24: Challenges in the game

- Effects

Effects are additions to objects, whether visual, audio or software. At the entrance to the clouds room, shown in Figure 25, there are two fire pillars. The fire effect has been added to them and their properties have been modified to suit the entrance. Additionally, the fire ignition sound effect has been added and its sound characteristics have been modified so that it only plays when approaching the entrance.

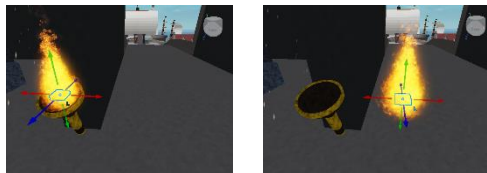


Figure 25: Add a fire effect

The game features various software effects, including the ability to run quickly by pressing the 'Shift' button, a programming file to allow the character to jump twice consecutively in mid-air, and a software file to enable swimming in the game's sea.

- Non-player character (NPC)

The game includes various non-player characters (NPCs) that the player does not control, such as portal characters, arms dealers, a shark, and characters in the clouds room and monsters in the second world.

C. Game Execution

To access the game, use the Roblox Player application from the official website. Select the desired game or search for it using the search bar. For the 'RSM game', either enclose the name in quotation marks or use the QR code shown in Figure 26. Finding the game by chance is difficult due to the large number of games on the platform.

The game features a unique icon, personally designed and shown in Figure27, as well as a custom cover, also displayed in Figure 28.

Figure 29 shows the game icon and cover. This is the login process.



Figure26: game's QR

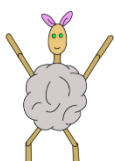


Figure27: Game icon

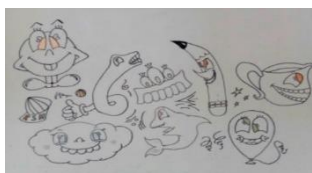


Figure28: Game cover

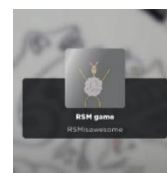


Figure29: Login to server

At the start of the game, the player emerges from the spawn portal into the first world. They can explore the world, drive cars, take boat rides, and swim in the sea, but must be cautious of sharks. Figure 30 displays various weapons stores, some of which are free while others require purchase. The boat and car are operated by touch.



Figure 30: Vehicles and weapons shop

To communicate with friends, form a team, and plan the battle, the player can access the chat function by pressing the button illustrated in Figure 31.

There is a castle located in the centre of the first world. The castle includes a clouds room, as shown in Figure 32.

In this room, there is a dish labelled 'The World of Clouds in Arabic', conceals a door. When touched, the door leads to the second world depicted in figure 33.



Figure 31: Chat button



Figure 32: Clouds room gate



Fig 33: second world Gate

In the second world, the player is taken to Weapons Island where they can collect equipment such as rifles, shells, and more as depicted in figure 34.

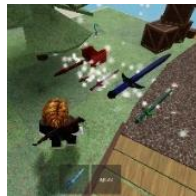


Figure 34: Weapons on Weapons Island

After preparing for the confrontation, the player travels to Monster Island. The only way to reach it is by travelling on small moving clouds. Figure 35 illustrates this. It is important to avoid falling down as there are small cloud balls that can cause death upon contact.

Upon arriving at Monsters Island, the player is immediately attacked by the cloud fairies using rain sprinklers. The player must avoid the attack and escape. As the player progresses, they encounter three spiders, each with a weak point. Although slow, the spiders can be defeated. In the final stage, the player confronts the boss, a swift samurai with a deadly strike and rapid regeneration upon death. Refer to figure 36 for a visual of all three monsters.



Figure 35: Moving clouds



Figure 36: Three main monsters

The developers intentionally designed the game with unresolved challenges and unfinished elements as a strategy to conceal production flaws and prolong the development process.

VII. CONCLUSION

Developing games on the Roblox platform using Lua is an interesting topic. This paper establishes that game development is not limited to high-specification devices. Novice developers can also create their own games without joining a specific development company. However, the success of development depends on the developer's programming and design experience. The greater the experience, the better the development. The developer must understand, assimilate and develop their skills and information as in figure 37.

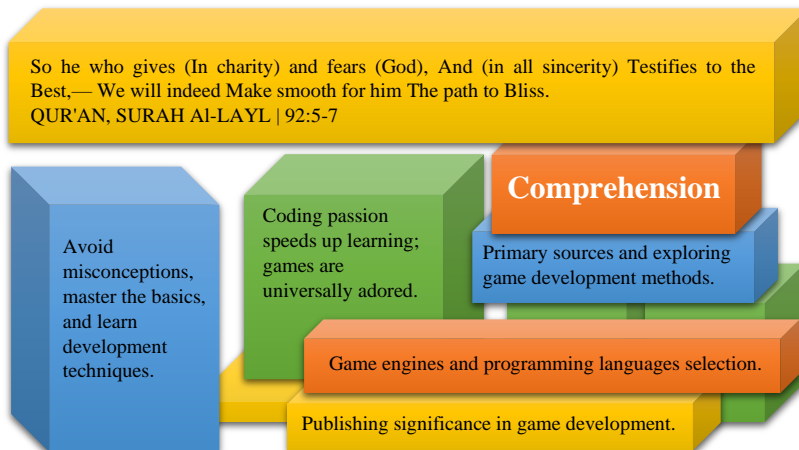


Figure 37: Development understanding requirements

Developers must remember that video game development is a creative and technical process that requires commitment and perseverance. The success and quality of the game increase as the developer's skills and knowledge in this exciting field improve. Therefore, developers should strive to enhance their skills and knowledge in this field.

REFERENCES

- [1] Á. Torres, "Game Development and Design: Principles and Practice," Paper presented at the University of La Frontera, June 15, 2023.
- [2] B. Keogh, "The Videogame Industry Does Not Exist: Why We Should Think Beyond Commercial Game Production," The MIT Press, 2023.
- [3] R. B. Jiwo and A. F. Aini, "Rancang Bangun Media Pembelajaran Berbasis Game menggunakan RPG Maker MV," Universitas Trunojoyo Madura, Indonesia, 2023.
- [4] G. B. Escorcía, "Game Online: Ancaman 'Candu Digital'," Syntax Idea, vol. 4, no. 12, pp. 1786-1795, 2022.
- [5] K. Khosiin, "Game Online: Ancaman 'Candu Digital'," Syntax Idea, vol. 4, no. 12, pp. 1786, 2022.
- [6] C. Meier, J. L. Saorín, A. Bonnet de León, and A. Guerrero Cobos, "Using the Roblox Video Game Engine for Creating Virtual tours and Learning about the Sculptural Heritage," International Journal of Emerging Technologies in Learning (iJET), vol. 15, no. 20, pp. 268, October 2020.
- [7] Y. Kou and X. Gui, "Harmful Design in the Metaverse and How to Mitigate it: A Case Study of User-Generated Virtual Worlds on Roblox," Proceedings of the ACM SIGCHI Conference on Designing Interactive Systems 2023 (DIS 2023), Pennsylvania State University, May 2023.
- [8] K. Alhasan, K. Alhasan, and S. Al Hashimi, "Roblox in Higher Education: Opportunities, Challenges, and Future Directions for Multimedia Learning," International Journal of Emerging Technologies in Learning (iJET), vol. 18, no. 19, pp. 32-46, 2023. University of Kent, University of Bahrain.
- [9] A. Tinterri, M.A. Guerriero, S. Annoscia, and A. Dipace, "Constructionism and game-making for learning in the age of Roblox: An analysis of current evidence and future perspectives," Italian Journal of Health Education, Sports, and Inclusive Didactics, vol. 7, no. 2, 2023. Edizioni Universitarie Romane.
- [10] A. Abilkaiyrkyzy, A. Elhagry, F. Laamarti, and A. El Saddik, "Metaverse Key Requirements and Platforms Survey," IEEE Access, vol. 11, pp. 117765-117787, 2023.

- [11] W. Ho and D. Lee, "Enhancing Engineering Education in the Roblox Metaverse: Utilizing chatGPT for Game Development for Electrical Machine Course," *International Journal on Advanced Science, Engineering & Information Technology*, vol. 13, no. 3, pp. 1052, 2023.
- [12] T. S. Sinar, M. A. Budiman, R. Ganie, and R. N. Rosa, "Students' Perceptions of Using Roblox in Multimodal Literacy Practices in Teaching and Learning English," *World Journal of English Language*, vol. 13, no. 7, pp. 146, 2023.
- [13] B. Berg Marklund, H. Engström, M. Hellkvist, and P. Backlund, "What Empirically Based Research Tells Us About Game Development," [Journal Name], vol. 8, no. 3, pp. 179-198, 2019.
- [14] Y. Ma, "Design of Serious Games for Teaching Industrial Engineering Methodologies: A Design Process Based on V-Model and an Application in Innovation Engineering," (PhD thesis in Industrial Engineering), Université Paris-Saclay, 2021.
- [15] D. Vagavolu, V. Agrahari, S. Chimalakonda, and A. S. M. Venigalla, "GE526: A Dataset of Open-Source Game Engines," in *Mining Software Repositories*, 2021, pp. 605-609.
- [16] W. Amaldoss and J. Du, "How Can Publishers Collaborate and Compete with News Aggregators?" *Journal of Communication*, vol. 60, no. 6, 2023.
- [17] C. McBride and G. Nakov, "Measuring with confidence: leveraging expressive type systems for correct-by-construction software," *Acta IMEKO*, vol. 12, no. 1, pp. 1-5, 2023.
- [18] É. Piette, D.J.N.J. Soemers, M. Stephenson, C.F. Sironi, M.H.M. Winands, and C. Browne, "Ludii - The Ludemic General Game System," *Frontiers in Artificial Intelligence and Applications*, vol. 325, pp. 411-418, 2020.
- [19] C. Martínez, C. Nicaud, and P. Rotondo, "Mathematical Models to Analyze Lua Hybrid Tables and Why They Need a Fix," arXiv:2208.13602v2 [cs.DM], 2023.
- [20] A. Vlasova, M. Tigina, I. Vlasov, A. Birillo, Y. Golubev, and T. Bryksin, "Programming language usage," in *Proceedings of the 19th International Conference on Mining Software Repositories (MSR '22)*, pp. 398-402.
- [21] A. Apicella, L.D. Lorenzo, F. Isgro, A. Pollastro, and R. Prevete, "Strategies to exploit XAI to improve classification systems," in *Proceedings of the 1st World*

- Conference on eXplainable Artificial Intelligence (xAI 2023), July 26-28, 2023, Lisboa, Portugal, arXiv:2306.05801 [cs.AI].
- [22] F. Luo, W. Yan, R. Liu, and M. Israel, "Elementary Students' Understanding of Variables in Computational Thinking-Integrated Instruction: A Mixed Methods Study," in SIGCSE 2022: Proceedings of the 53rd ACM Technical Symposium on Computer Science Education - Volume 1, pp. 523-529.
- [23] M. Chernoff, "Automatically removing widows and orphans with lua-widow-control," TUGboat, vol. 43, no. 1, pp. 28-39, 2022.
- [24] L. Maliang, L. Ma, D. Liu, and J. Li, "Lua-based method and a Lua-based device for obtaining a mobile phone application memory," published on June 11, 2019.
- [25] Korean Institute of Communications and Information Sciences, "Design and Implementation of a Volumetric Video Player based on Point Cloud," Journal of the Korean Institute of Communications and Information Sciences, vol. 47, no. 10, pp. 1,660-1,668, 2022.